A minimal model for solvent evaporation and absorption in thin films

Matthew G. Hennessy[a,*], Giulia L. Ferretti[a], João T. Cabral[a], Omar K. Matar[a,*]

[a]*Department of Chemical Engineering, Imperial College London, South Kensington Campus, London, SW7 2AZ, United Kingdom*

Abstract

We present a minimal model of solvent evaporation and absorption in thin films consisting of a volatile solvent and non-volatile solutes. An asymptotic analysis yields expressions that facilitate the extraction of physically significant model parameters from experimental data, namely the mass transfer coefficient and composition-dependent diffusivity. The model can be used to predict the dynamics of drying and film formation, as well as sorption/desorption, over a wide range of experimental conditions. A state diagram is used to understand the experimental conditions that lead to the formation of a solute-rich layer, or "skin", at the evaporating surface during drying. In the case of solvent absorption, the model captures the existence of a saturation front that propagates from the film surface towards the substrate. The theoretical results are found to be in excellent agreement with data produced from dynamic vapour sorption experiments of ternary mixtures comprising an aluminum salt, glycerol, and water. Moreover, the model should be generally applicable to a variety of practical contexts, from paints and coatings, to personal care, packaging, and electronics.

Keywords:
Thin films, evaporation, sorption, desorption, diffusion, skin formation, saturation front, mathematical model, asymptotic analysis

1. Introduction

Thin evaporating films that are composed of a volatile solvent and non-volatile solutes play an important role in a broad spectrum of applications ranging from paints and coatings [1, 2], ink-jet printing [3], and flexible electronics [4]. Over the last decade, theoretical and experimental advances in film drying have led to innovative and cost-effective techniques for manufacturing multifunctional materials via evaporative self-assembly [5] and lithographic processes [6, 7, 8], which, under certain conditions, result in the stratification of mixture components in the direction that is normal to the film surface. This stratification can be advantageous in the case of scratch-resistant coatings [9] or detrimental in the case of drying, where it can lead to warping, wrinkling, or cracking [10, 11]. An equally relevant process is the absorption of solvent from the surrounding environment by a dry film or matrix. This plays a crucial role in the controlled release of pharmaceuticals [12], food science [13], and personal care products such as anti-perspirants [14].

In all of the aforementioned technologies, quantitative and predictive understanding of solvent evaporation and absorption in thin films is essential. Thus, a number of theoretical studies have been carried out to which aim to develop models of these processes [15]. In the case of film drying, Eckersley & Rudin [16] derived a simple model that can account for two key stages that are often observed in experiments. The first of these is the constant-rate period, whereby evaporative mass loss takes place at a uniform rate over time. This is followed by the falling-rate period, where mass loss slows due to the depletion of the volatile species. Remarkably, Eckersley & Rudin's model is able to capture these two stages without explicitly considering the spatial variation of the film composition. Extended models that are based on the diffusion equation [17, 18, 19, 20] have been used to study concentration gradients throughout the film and, in particular, the onset of viscous or brittle solute-rich skins below the free surface [21, 22]. The formation of a skin is expected to occur when the depleted solvent cannot be replenished sufficiently quickly due to local decreases in the rate of mass diffusion. Detailed models based on thermodynamic principles have been proposed as a means of accurately describing the transport of heat and mass during the drying process [23, 24, 25]. Finally, there is a wide body of literature concerning the application of hydrodynamic models to the problem of film drying [26, 27]. These models explicitly account for the motion of the liquid phase and have been used to understand flow-driven solute deposition, e.g., the coffee-stain effect [28, 29, 30, 31]; skin formation [32, 33]; and the onset of Marangoni instabilities caused by composition gradients at the evaporating surface [34, 35, 36, 37, 38].

In the particular case of polymeric films, the problem

*Corresponding authors
Email addresses: m.hennessy@imperial.ac.uk (Matthew G. Hennessy), giulia.ferretti08@imperial.ac.uk (Giulia L. Ferretti), j.cabral@imperial.ac.uk (João T. Cabral), o.matar@imperial.ac.uk (Omar K. Matar)

of theoretically describing the absorption of solvent has received considerable attention due to the possibility of non-Fickian diffusion in these systems [39]. Several models have been proposed which aim to couple the diffusion of absorbed solvent throughout the film with the elastic [40, 41, 42] or viscoelastic [43, 44, 45, 46] response of the polymer network. Simplifications of these models that neglect the detailed mechanics of the polymer matrix have been proposed in the context of drug delivery [47, 48, 49].

The extensive detail of existing models [50, 51, 52] for solvent evaporation and absorption in thin films has enabled a wealth of insight to be gained into these technologically relevant processes. However, the complexity of these models can restrict their practical use, since sophisticated computational methods and a large number of parameters may be required to solve the governing equations and hence make theoretical predictions. Therefore, the goal of this paper is to develop a practical and efficient approach to modelling solvent evaporation and absorption in thin films. Our approach is based on a "minimal" descriptive model that contains a limited number of physically meaningful parameters, which can be linked to key experimental observables, and is robust enough to be used as a predictive tool. Novel analytical expressions are derived from the model and used to systematically extract parameter values from experimental data.

The predictive capability of the model is achieved by requiring it to have a minimal number of "inputs", namely the initial film composition and the time evolution of the film thickness (or film mass). A simple fitting procedure will then "output" values for the remaining physical parameters. Based on these parameters, the model can subsequently make quantitative predictions about the drying and absorption processes, including skin formation, as the system conditions, e.g., the initial film compositions or thicknesses, are varied. An overview of how the model can be applied to the problem of film drying is illustrated in Figure S1. To verify that the model is able to accurately capture film drying and solvent absorption, we compare theoretical predictions of the film thickness to experimental data produced from dynamic vapour sorption experiments using ternary mixtures of a salt, humectant, and water. The agreement between theory and experiment is found to be excellent.

2. Model formulation

We consider the behaviour of a mixture consisting of a volatile solvent and one or more non-volatile solutes. The mixture forms a long layer on top of a horizontal and non-permeable substrate, as illustrated in Figure 1. The surface tension of the mixture is assumed to be sufficiently strong that deformations in the film surface from the flat state can be neglected; thus, the finite thickness of the film can be described by a function of time $h(t)$. Depending on the atmospheric conditions above the film surface, solvent can either evaporate from the film, causing a decrease in the thickness, or be absorbed from the atmosphere, leading to an increase in the film thickness. We refer to these as the "drying" and "sorption" problems, respectively. In evaporating systems with large solvent excess, the drying problem effectively describes film formation.

To simplify the mathematical description of the drying and sorption problems, a number of assumptions about the system are made. Diffusion is assumed to be the sole means of mass transport within the bulk and adequately described using Fick's law with a composition-dependent diffusivity D. We do not consider convective transport or any hydrodynamic effects. The exchange of solvent with the atmosphere is described using a phenomenological mass flux J that must balance the diffusive flux at the film surface. Any temperature changes, such as those resulting from evaporative cooling, are assumed to be sufficiently small that the system can be treated as isothermal. Furthermore, due to the large horizontal extent of the film in comparison to its initial height, the system is treated as one dimensional. Finally, we make the important assumption that the density differences between the solvent and solutes are negligibly small so that the mixture density can be taken as constant.

Under these assumptions, conservation of solvent in one dimension leads to a nonlinear diffusion equation for the solvent fraction ϕ given by

$$\frac{\partial \phi}{\partial t} = \frac{\partial}{\partial z}\left[D(\phi)\frac{\partial \phi}{\partial z}\right], \tag{1}$$

where z denotes the vertical distance from the substrate. In this problem, the mass and volume fractions are interchangeable due to the assumption that the mixture has a constant density ρ. Furthermore, the quantity $1-\phi$ corresponds to the combined fraction of non-volatile solutes, effectively reducing the problem to a "pseudo-binary" system. A complete ternary description is then recovered by the explicit dependence of the model parameters on the ratio of non-volatile species. To capture the general trend of the diffusivity of solvent decreasing in regions of increasing solute, we assume that D has a simple functional form given by

$$D(\phi) = (D_0 - D_\infty)\phi^a + D_\infty, \tag{2}$$

where D_0 and D_∞ represent the effective diffusion coefficients in "wet" (solvent-rich) and "dry" (solute-rich) layers, respectively, and the exponent a is a fitting parameter.

The form of the diffusivity given by (2) is expected to be well suited for describing glass-forming systems that exhibit a near-constant diffusion coefficient below the glass transition [53]. For polymer systems that remain above the glass transition, several exponential forms for D have been proposed based on phenomenology [54, 55] or derived from free-volume theory [56, 57]. Exponential forms of D will tend to zero as $\phi \to 0$ much faster than the polynomial form of (2) with $D_\infty = 0$, leading to differences in the diffusion-limited regimes of solvent absorption and evaporation. However, these differences will only be substantial

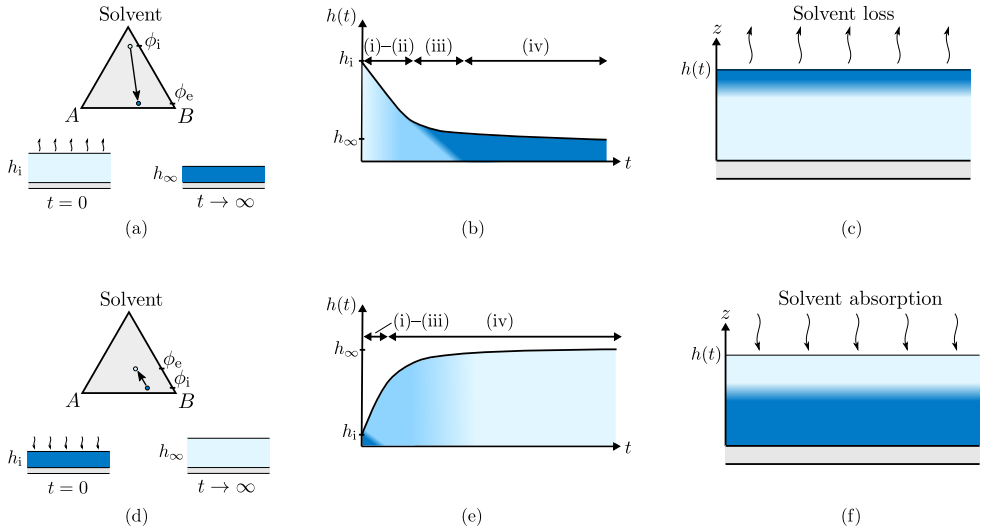


Figure 1: (Color online) Schematic diagrams of solvent evaporation [(a)–(c)] and absorption [(d)–(f)] in mixtures composed of a volatile solvent and non-volatile solutes. Increasing darkness corresponds to decreasing solvent fraction. The mixtures form thin films on top of a non-permeable substrate. Typical pathways through the phase diagram during solvent removal (a) and absorption (d) in the case of a ternary mixture. The initial and equilibrium solvent fractions are denoted by ϕ_i and ϕ_e, respectively. The evaporation process can be decomposed into four main stages (b); the first two describe the constant-rate period whereby the decrease in film thickness is approximately linear with time. The third and fourth correspond to the falling-rate period, in which the rate of thinning decreases due to the formation of a solute-rich skin near the surface of the film (c). This skin inhibits the transport of fresh solvent to the film surface. Similarly, the absorption process has four key stages (e); the first three correspond to onset of a saturation front that propagates from the film surface towards the substrate (f) and the last describes the expansion of the film to its steady state.

if the diffusion-limited regime is entered early in the drying problem, or is prolonged in the sorption problem. The polynomial form (2) is otherwise expected to be an adequate representation of the diffusivity for general systems. By considering the detailed interactions between the solvent and solute(s), it is also possible to derive functional forms for the diffusivity that can account for elastic effects [58] and maximum packing of solute [17, 20]. However, we refrain from incorporating additional physics into the model in order to retain its simplicity.

At the non-permeable substrate located at $z = 0$, we impose a no-flux boundary condition given by

$$\frac{\partial \phi}{\partial z} = 0, \quad z = 0. \tag{3}$$

To derive boundary conditions at the film surface located at $z = h(t)$, we use the fact the only the solvent can exchange mass with the surrounding atmosphere. By letting J denote the volume flux of solvent through the film surface, conservation of solute and solvent gives, respectively,

$$-D(\phi)\frac{\partial(1-\phi)}{\partial z} - (1-\phi)\frac{\mathrm{d}h}{\mathrm{d}t} = 0, \qquad z = h(t), \tag{4a}$$

$$-D(\phi)\frac{\partial \phi}{\partial z} - \phi\frac{\mathrm{d}h}{\mathrm{d}t} = J(\phi), \quad z = h(t). \tag{4b}$$

The terms that are proportional to $\mathrm{d}h/\mathrm{d}t$ account for the fact that each mass balance in (4) holds across a moving surface. We will use the convention that $J < 0$ and $J > 0$ correspond to solvent entering and leaving the film, respectively. By adding the two boundary conditions in (4), a differential equation for the film thickness is obtained:

$$\frac{\mathrm{d}h}{\mathrm{d}t} = -J(\phi(h(t), t)). \tag{5}$$

Inserting (5) into (4b) yields a simplified boundary condition for the diffusive flux of solvent:

$$-D(\phi)\frac{\partial \phi}{\partial z} = (1-\phi)\,J(\phi), \quad z = h(t). \tag{6}$$

For the rest of the paper, the conditions (5) and (6) will be used in place of (4). We choose a simple form of the solvent flux [59, 60, 61, 54] given by

$$J = k[\phi(h(t), t) - \phi_e], \tag{7}$$

where ϕ_e is equilibrium solvent fraction and k is a mass transfer coefficient. By invoking thermodynamic principles [57, 62, 63, 50], it is possible to derive nonlinear relationships between the flux J and the solvent fraction ϕ. As shown in Section S2 of the Supplementary Material, a nonlinear flux does not lead to substantial changes in the drying problem. However, significant quantitative discrepancies can arise in the sorption problem. It is important to emphasize that the qualitative features of the dynamics remain unchanged, and the asymptotic approach that is developed for the model based on the simplified flux (7) can also be applied to the case of a nonlinear flux. Implications for the accurate description of common film drying processes are discussed in Section 5.

To close the model, initial conditions must be prescribed. We assume that the film is initially well mixed,

corresponding to spatially uniform distributions of solvent and solute. Thus, the initial conditions for the system can be written as

$$\phi(z,0) \equiv \phi_\mathrm{i}, \quad h(0) = h_\mathrm{i}, \tag{8}$$

where the initial solvent fraction ϕ_i is a constant and h_i denotes the initial thickness of the film.

A useful identity can be derived by integrating (1) over the thickness of the film and making use of (4b) and (5), leading to

$$\int_0^{h(t)} \phi(z,t)\,\mathrm{d}z = h(t) - (1-\phi_\mathrm{i})h_\mathrm{i}. \tag{9}$$

Equation (9) can be used to relate the total mass of solvent in the film to its thickness and thus shows that these two quantities are interchangeable. We will see below that, despite the model being based on Fickian diffusion, sorption does not necessarily lead to film thicknesses, and hence film masses, that scale like the square root of time.

2.1. Non-dimensionalisation

The model is cast into non-dimensional form in order to identify the key parameter regimes. Tildes denote the dimensionless counterpart of a dimensional variable. The vertical coordinate z is written in terms of the initial film height so that $z = h_\mathrm{i}\tilde{z}$. Time is written in terms of the time scale of mass transfer, leading to $t = (h_\mathrm{i}/k)\tilde{t}$. Finally, the diffusivity is written as $D(\phi) = D_0\tilde{D}(\phi)$, where

$$\tilde{D}(\phi) = (1-\delta)\phi^a + \delta \simeq \phi^a + \delta, \tag{10}$$

with $\delta = D_\infty/D_0 \ll 1$ being the ratio of dry to wet diffusivities. A Péclet number, Pe, for this system can be defined as

$$\mathrm{Pe} = kh_\mathrm{i}/D_0, \tag{11}$$

which represents the ratio of the diffusive time scale $\tau_\mathrm{diff} = h_\mathrm{i}^2/D_0$ to the time scale of mass transfer, $\tau_\mathrm{mt} = h_\mathrm{i}/k$. It is important to emphasise that the Péclet number as defined in (11) does not give a true representation of whether diffusion will be fast or slow compared to solvent evaporation/absorption because the diffusivity can change by several orders of magnitude as the solvent fraction changes from ϕ_i to ϕ_e due to its dependence on the local film composition.

Upon dropping the tildes, the non-dimensional diffusion equation is given by

$$\mathrm{Pe}\,\frac{\partial\phi}{\partial t} = \frac{\partial}{\partial z}\left[D(\phi)\frac{\partial\phi}{\partial z}\right], \tag{12a}$$

which has boundary conditions

$$\frac{\partial\phi}{\partial z} = 0, \qquad z = 0, \tag{12b}$$

$$-D(\phi)\frac{\partial\phi}{\partial z} = \mathrm{Pe}\,(1-\phi)(\phi-\phi_\mathrm{e}), \quad z = h(t). \tag{12c}$$

The film thickness evolves according to

$$\frac{\mathrm{d}h}{\mathrm{d}t} = -[\phi(h(t),t) - \phi_\mathrm{e}]. \tag{12d}$$

The initial conditions are

$$\phi = \phi_\mathrm{i}, \quad h = 1, \quad t = 0. \tag{12e}$$

The integral (9) in dimensionless form reads

$$\int_0^{h(t)} \phi(z,t)\,\mathrm{d}z = h(t) - 1 + \phi_\mathrm{i}. \tag{12f}$$

The steady-state film thickness, h_∞, can be readily deduced from (12f) using the fact that $\phi \to \phi_\mathrm{e}$ as $t \to \infty$; this yields

$$h_\infty = \frac{1-\phi_\mathrm{i}}{1-\phi_\mathrm{e}}. \tag{13}$$

The relationship in (13) provides a simple way to infer either ϕ_e or ϕ_i from experimental measurements of the equilibrium film thickness.

The dimensionless model (12) will now be analysed using a combination of asymptotic and numerical methods; details of the computational scheme are given in Section S3 of the Supplementary Material.

3. Film drying

We first consider the scenario of complete drying by setting $\phi_\mathrm{e} = 0$ in the governing equations. The alternative case when $\phi_\mathrm{e} > 0$ is discussed in Section 3.1.5. The analysis of drying can be split into two parts depending on whether the rate of evaporation is fast or slow compared to the initial rate of diffusion. The relative rate of these two processes is characterised by the initial Péclet number, $\varepsilon \equiv \mathrm{Pe}\,\phi_\mathrm{i}^{-a}$, where the factor of ϕ_i^a accounts for the initial value of the diffusivity, i.e., $D \sim \phi_\mathrm{i}^a$ at $t = 0$. We first assume that the initial composition of the film is such that the initial Péclet number is small, $\varepsilon \ll 1$, thus implying $\phi_\mathrm{i} \gg \mathrm{Pe}^{1/a}$. We refer to this as "solvent-rich" drying. We briefly consider "solute-rich" drying, characterised by $\phi_\mathrm{i} = O(\mathrm{Pe}^{1/a})$ or smaller, in Section 3.2.

3.1. Solvent-rich drying

We assume that $\varepsilon \ll 1$ and $\delta \ll \mathrm{Pe}$. The first inequality defines the case of solvent-rich drying. The second inequality is not essential but it will facilitate a discussion of all of the key drying stages, of which there are four. Three of these stages are illustrated in Figure S3; the fourth and final stage can be considered a sub-stage of the third. The four stages essentially arise from the different balances that occur between the left- and right-hand sides of the diffusion equation (12a), which themselves are caused by the decrease in the diffusivity during the drying process. Thus, plotting the diffusivity as a function of the solvent fraction enables the onset and transition between

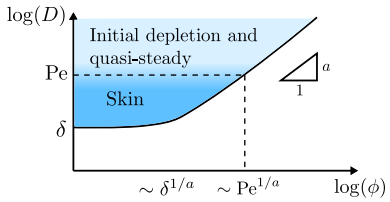


Figure 2: (Color online) A state diagram of the drying process can be created by plotting the (dimensionless) diffusivity as a function of the solvent fraction. By tracing out the path along the curve starting from $\phi = \phi_\mathrm{i}$ and ending at $\phi = \phi_\mathrm{e}$, the different stages that will occur during drying can be predicted.

various drying stages to be visualised, as shown in Figure 2. The drying dynamics can be understood by tracing out the path along the diffusivity curve starting from the initial value of the solvent fraction ϕ_i and ending at ϕ_e, which we take as zero for now. The evolution of the film thickness across the drying stages is illustrated in Figure 1 (b).

A detailed mathematical analysis of each drying stage is given in Section S4 of the Supplementary Material. We now summarise these stages and present the key results that are relevant for film drying experiments.

3.1.1. Stage (i): Initial depletion

The first drying stage is characterised by $t = O(\varepsilon)$ with $\mathrm{Pe}^{1/a} \ll \phi \leq \phi_\mathrm{i}$ and it describes the dynamics on the diffusive time scale. Here, the initial depletion of solvent from the film surface leads to the formation of a compositional boundary layer that grows in thickness until it reaches the substrate. The film thickness in this stage is given by $h(t) \sim 1 - \phi_\mathrm{i} t$, which is valid for $t \sim \varepsilon \ll 1$. Due to the slow rate of evaporation on the diffusive time scale, the decrease in film height is negligible, making this stage difficult to detect in experimental measurements of the film thickness.

3.1.2. Stage (ii): Quasi-steady

The second stage is characterised by $t = O(1)$ with $\mathrm{Pe}^{1/a} \ll \phi < \phi_\mathrm{i}$ and describes the dynamics on the evaporative time scale. Diffusion is sufficiently fast that concentration gradients across the film are small. The solvent fraction evolves quasi-steadily as evaporation thins the film.

Stage (ii) is captured by writing $\phi = \phi_\mathrm{i}\bar{\phi}$ in the dimensionless model (12). Taking $\varepsilon \to 0$ then yields a leading-order solvent fraction, $\bar{\phi}_0$, that is uniform in space, which can be used to show that the film thickness in this stage is given by the implicit expression

$$h_0(t) + (1 - \phi_\mathrm{i}) \log\left[\frac{h_0(t) - 1 + \phi_\mathrm{i}}{\phi_\mathrm{i}}\right] + t = 1. \qquad (14)$$

The leading-order solution for the film thickness (14) describes the complete thinning of the film to its equilibrium thickness in the absence of concentration gradients. Furthermore, the analysis indicates that, to leading order, the drying kinetics in stage (ii) are solely determined by the form of the evaporative flux and thus the rate of thinning is set by the time scale of evaporation $\tau_\mathrm{evap} = h_\mathrm{i}/k$. A comparison of film thicknesses computed from the leading-order solution (14) and a numerical simulation of the full model (12) is shown in Figure 3. The leading-order solution appears to do an excellent job at capturing the entire drying process and, in particular, the constant-rate period. However, a closer inspection of the final drying stage (see the inset of Figure 3) shows that there is a retardation of the drying process, which the leading-order solution (14) is unable to capture. This retardation is caused by the formation of a solute-rich skin at the surface of the film, details of which are presented in the Supplementary Material. Nevertheless, the leading-order solution (14) can be used in practice as a means of extracting τ_evap by fitting this curve to experimental data in the constant-rate period of drying.

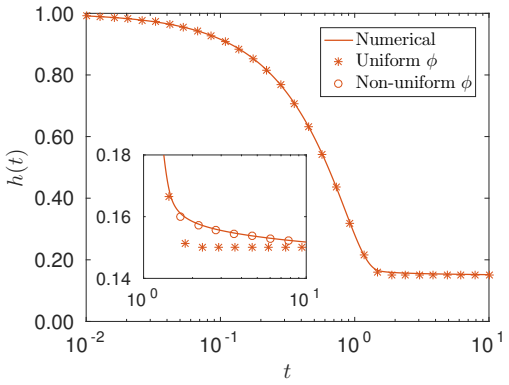


Figure 3: (Color online) Evolution of the film thickness during film drying. Lines correspond to numerical simulations. Stars and circles correspond to the asymptotic solution in stages (ii) and (iii)–(iv), respectively. Parameters are $\phi_\mathrm{i} = 0.85$, $\mathrm{Pe} = 10^{-2}$, $\delta = 10^{-5}$, $\phi_\mathrm{e} = 0$, and $a = 3$.

3.1.3. Stage (iii): Skin formation

The third stage of drying captures the formation of a solute-rich skin and is defined by $t = O(1)$ with $\delta^{1/a} \ll \phi = O(\mathrm{Pe}^{1/a})$. At this stage, enough solvent has been removed to induce a large change in the diffusivity, leading to the time scales of evaporation and diffusion becoming commensurate. A large gradient in the solvent fraction forms near the film surface because diffusion becomes too slow to replenish depleted solvent. This composition gradient corresponds a skin. The lack of solvent near the surface leads to a substantial decrease in the rate of drying.

The transition between stages (ii) and (iii) occurs when the magnitude of the solvent fraction is $\phi \sim \mathrm{Pe}^{1/a} \ll 1$, the film thickness is

$$h \sim (1 - \phi_\mathrm{i})(1 + \mathrm{Pe}^{1/a}), \qquad (15)$$

and can be experimentally identified as the point where the leading-order solution (14) begins to significantly deviate

from experimental data. In Figure 3, the stage (ii)–(iii) transition can be seen when $t \sim 1.5$.

The circles in the inset of Figure 3 denote the film thickness that is computed from a numerical simulation of the asymptotically reduced model in this stage. The solution is able to capture the decrease in the rate of thinning that the leading-order solution in stage (ii), given by (14) and shown as stars, could not.

The asymptotically reduced model in this stage depends on two dimensionless parameters: a and δ. Numerical simulations of the full model (12) are used to explore how the parameters a and δ influence the long-term evolution of the film thickness. Figure 4 (a) focuses on the role of a with δ fixed. As predicted from the analysis of stages (i) and (ii), the initial evolution of the film thickness is the same for all values of a [see, e.g., (14)] and follows the quasi-steady evolution corresponding to $a = 0$ (constant diffusivity). However, since the parameter a controls how sharply the diffusivity decreases with the solvent fraction, it also sets the time at which skin formation occurs and the thinning rate slows. Interestingly, the long-term thinning rate approaches a constant value (on a semi-log plot) that is independent of a. Figure 4 (b) shows the influence of δ for fixed a, and reveals that the dry diffusivity δ selects the final rate of film thinning, which can understood by analysing the long-term dynamics that occur in the fourth and final drying stage.

3.1.4. Stage (iv): Final drying

The fourth and final drying stage is entered when the solvent fraction is sufficiently small that the diffusivity can be treated as constant; this occurs when $\phi \ll \delta^{1/a}$ and $t \gg 1$. The governing equations in stage (iv) are linear and can be solved using a Fourier series. The solution for the film thickness can be used to show that the final rate of thinning is given by

$$\frac{\mathrm{d}}{\mathrm{d}t}\left[\log(h(t) - h_\infty)\right] \sim -(1-\phi_\mathrm{i})^{-1}\lambda_0^2\breve{\delta}, \tag{16}$$

where $\breve{\delta} = \mathrm{Pe}^{-1}(1-\phi_\mathrm{i})^{-1}\delta$ and λ_0 is the smallest positive root of

$$\lambda_0 \tan\lambda_0 = \breve{\delta}^{-1}. \tag{17}$$

Equation (16) suggests that a convenient method for experimentally measuring the combination $\lambda_0^2\breve{\delta}$ is by plotting $\log(h - h_\infty)$, where $h_\infty = 1 - \phi_\mathrm{i}$ when $\phi_\mathrm{e} = 0$, and then calculating the slope of the curve near the end of the drying process. Once $\lambda_0^2\breve{\delta}$ is known, the physically relevant value of $\breve{\delta}$ can be isolated by solving (17). Details of this procedure will be given in Section 5.1.

The dashed lines in Figure 4 represent the long-term thinning rates that are predicted from (16), all of which are asymptotically approached by the numerical solutions of the full model (12). The numerical solutions are seen to tend more rapidly to the asymptotic thinning rate (16) for larger values of δ; this is due to the condition defining stage (iv), i.e., $\phi \ll \delta^{1/a}$, being satisfied earlier in the drying process.

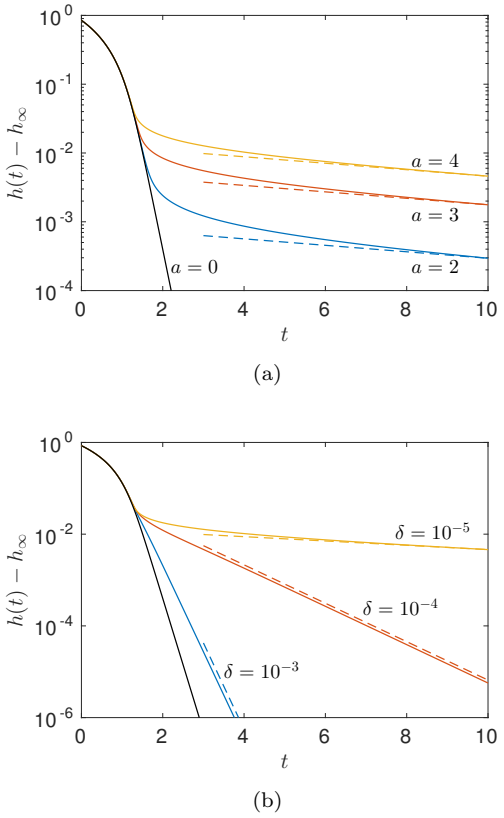


Figure 4: (Color online) The influence of the dimensionless diffusivity $D(\phi) = \phi^a + \delta$ on the evolution of the film thickness when a varies (a) and when δ varies (b). The solid lines correspond to numerical simulations and the dashed lines denote the long-term drying rate as calculated from (16). Parameters are $\mathrm{Pe} = 10^{-2}$, $\phi_\mathrm{i} = 0.85$, and $\phi_\mathrm{e} = 0$. In panel (a), we have set $\delta = 10^{-5}$; in panel (b), we take $a = 4$. In both cases, $h_\infty = 1 - \phi_\mathrm{i}$.

3.1.5. Incomplete drying

Analysing the case of incomplete drying, whereby $\phi_\mathrm{e} > 0$, is relatively straightforward. In essence, the parameter ϕ_e selects the final stage of the drying process; see Figure 2. If $\phi_\mathrm{e} \gg \mathrm{Pe}^{1/a}$, then the system always evolves quasi-statically and the formation of a skin can be avoided. In this case, the equation governing the (dimensionless) film thickness can be written as

$$\frac{\mathrm{d}h}{\mathrm{d}t} = -(1-\phi_\mathrm{e}) + \frac{1-\phi_\mathrm{i}}{h}, \tag{18}$$

which satisfies $h(0) = 1$. However, when $\phi_\mathrm{e} \ll \mathrm{Pe}^{1/a}$, skin formation is very likely. If $\delta^{1/a} \ll \phi_\mathrm{e} \ll \mathrm{Pe}^{1/a}$, then only drying stages (i)–(iii) will be entered, whereas all four stages will occur if $\phi_\mathrm{e} \ll \delta^{1/a}$.

3.2. Drying of a solute-rich film

If the film is initially rich in solute, i.e., if $\phi_\mathrm{i} = O(\mathrm{Pe}^{1/a})$ or smaller, then the system begins to dry from stage (iii) or (iv), leading to instant skin formation.

4. Film sorption

The non-dimensional model (12) can also describe the situation whereby a film absorbs solvent from the surrounding atmosphere. We first analyse the case of a dry film absorbing solvent by setting $\phi_\mathrm{i} = 0$ and $\phi_\mathrm{e} > 0$. The case when $\phi_\mathrm{i} \neq 0$ will be discussed in Section 4.1.2. The solvent fraction is rescaled according to $\phi = \phi_\mathrm{e}\Phi$ so that $\Phi = 1$ corresponds to the equilibrium saturation. In this case, the diffusivity can be written as $\mathcal{D}(\Phi) = \Phi^a + \Delta$, with $\Delta = \delta\phi_\mathrm{e}^{-a}$ being a key parameter of the model.

Similar to the drying problem, there are two sorption regimes; these are based on the magnitude of the equilibrium Péclet number $\epsilon \equiv \mathrm{Pe}\,\phi_\mathrm{e}^{-a}$, where the factor of ϕ_e^{-a} accounts for the value of the diffusivity at equilibrium, $D \sim \phi_\mathrm{e}^a$ as $t \to \infty$. If $\epsilon \gg 1$, corresponding to $\phi_\mathrm{e} \ll \mathrm{Pe}^{1/a}$, then the increase in diffusivity as the film absorbs solvent is not sufficiently large to make absorption the rate-limiting process. That is, the time scale of diffusion is always much greater than that of absorption when $\epsilon \gg 1$. However, if $\epsilon \ll 1$, corresponding to $\phi_\mathrm{e} \gg \mathrm{Pe}^{1/a}$, then the film becomes sufficiently saturated that the diffusive time scale falls below that of solvent absorption. We refer to the $\epsilon \ll 1$ ($\phi_\mathrm{e} \gg \mathrm{Pe}^{1/a}$) and $\epsilon \gg 1$ ($\phi_\mathrm{e} \ll \mathrm{Pe}^{1/a}$) cases as "strong" and "weak" saturation, respectively.

4.1. Strong saturation

We begin by considering the case when the saturation is strong, i.e., when $\epsilon \equiv \mathrm{Pe}\,\phi_\mathrm{e}^{-a} \ll 1$. To elucidate all of the key stages in this limit, the additional assumptions that $\Delta \ll \epsilon$ and $a > 1$ are made. There are four stages that can be considered, the mathematical details of which are presented in Section S5 of the Supplementary Material. The evolution of the film thickness and solvent fraction across these stages is illustrated in Figure 1 (e) and Figure 5, respectively. In summary, the four sorption stages are:

i. *Initial saturation* $t \ll \epsilon^{1/(a+1)}$ and $\Phi \ll \Delta^{1/a}$: This describes the initial saturation of the film which is confined to a thin layer near the surface of width $O(\Delta^{(1/a)+1}\epsilon^{-1})$.

ii. *Saturation front* $t = O(\epsilon^{1/(a+1)})$ and $\Phi = O(\epsilon^{1/(a+1)})$: The surface becomes sufficiently saturated with solvent to induce large increases in the diffusivity. The rapid flow of solvent from regions of high diffusivity (the film surface) to low diffusivity (the bulk) leads to the onset of a diffuse saturation front, centred about $z = s(t)$, that propagates from the surface of the film towards the substrate. This saturation front separates regions of the film that are dry, $\Phi \sim 0$ for $z < s(t)$, from regions that are partially saturated, $\Phi > 0$ for $z > s(t)$.

iii. *Transition* $\epsilon^{1/(a+1)} < t \ll 1$ and $\epsilon^{1/(a+1)} < \Phi \ll 1$: The saturation front reaches the substrate and the solvent fraction begins tending towards a spatially uniform state due to the fast rate of diffusion. The expansion of the film is negligible up to this point, meaning stages (i)–(iii) are unlikely to be detectable in experimental measurements of the film thickness.

iv. *Quasi-steady* $t = O(1)$ and $\Phi = O(1)$: Newly absorbed solvent is rapidly and uniformly distributed throughout the film, leading to a solvent fraction that evolves in a quasi-steady manner. The increase in volume is sufficiently large to induce $O(1)$ changes in the film thickness. The film, therefore, expands until its equilibrium thickness is reached.

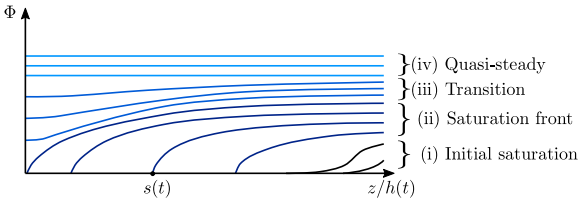


Figure 5: (Color online) The dynamics of solvent absorption in the limit of strong saturation, $\epsilon \equiv \mathrm{Pe}\,\phi_\mathrm{e}^{-a} \ll 1$. There are four key stages to consider.

We present the key results from analysing stage (iv), which are pertinent to film sorption experiments.

4.1.1. Stage (iv): Quasi-steady

In this stage, the time scale of diffusion is much faster than that of solvent absorption; thus, at each point in time, the solvent appears to be in a steady-state profile. We find that the leading-order solution for the solvent fraction in stage (iv) is uniform in space, which can be used to show that the film thickness is given by the implicit expression

$$h_0 - 1 + \frac{1}{1-\phi_\mathrm{e}} \log\left[\frac{1-(1-\phi_\mathrm{e})h_0}{\phi_\mathrm{e}}\right] = -(1-\phi_\mathrm{e})t. \quad (19)$$

If the equilibrium solvent fraction is small, $\phi_\mathrm{e} \ll 1$, then the leading-order film thickness (19) can be simply written as

$$h_0(t) = 1 + \phi_\mathrm{e}(1 - \mathrm{e}^{-t}) + O(\phi_\mathrm{e}^2). \quad (20)$$

Taking $t \to \infty$ in (20) shows that the steady-state film thickness in the limit of small solvent absorption is given by $h_0 \to 1 + \phi_\mathrm{e}$, which are the first two terms in the small-ϕ_e expansion of the true equilibrium thickness, $h_\infty = (1-\phi_\mathrm{e})^{-1} = 1 + \phi_\mathrm{e} + O(\phi_\mathrm{e}^2)$. The form of (20) suggests that in the limit $\phi_\mathrm{e} \ll 1$, all experimental data should collapse onto a master curve given by

$$\phi_\mathrm{e}^{-1}(h_0 - 1) = 1 - \mathrm{e}^{-t}. \quad (21)$$

Fitting experimental data to either (20) or (21) will provides a simple means of extracting the time scale of absorption, h_i/k, and thus deducing a value for the mass transfer coefficient k.

A comparison of the asymptotic solution for the film thickness given by (19) with a numerical solution of the

full model (12) is shown in Figure S8. The exceptional agreement between these two solutions provides verification that, despite the complicated dynamics that occur in stages (i)–(iii), the film thickness is mainly driven by the relatively simple quasi-steady dynamics of stage (iv). This fact has significant experimental implications: since diffusion is a higher-order effect and does not enter the leading-order solutions for the film thickness, tracking the evolution of the film height in absorption experiments in the strong-saturation limit will provide limited information on the values of the wet and dry diffusivities, D_0 and D_∞, respectively, as well as the diffusivity exponent a.

Had we assumed that $\epsilon \ll \Delta$, then the time scale of diffusion, even at $t = 0$, would be faster than absorption and thus the entire process would be described by stage (iv). Similarly, if $0 < a < 1$, then the rapid initial increase of the diffusivity leads to stage (iv) being entered almost immediately.

4.1.2. Absorption by a pre-saturated film

The initial solvent fraction, ϕ_i, plays only a minor role in the sorption problem; it selects which of the four stages the evolution of the system begins from. The overall increase in the diffusivity of a pre-saturated film means that the solvent fraction more rapidly approaches a quasi-steady state compared to if the film was initially completely dry. Thus, by assuming that the solvent fraction evolves quasi-steadily, we find that $\Phi \sim \phi_\mathrm{e}^{-1}[1-(1-\phi_\mathrm{i})/h]$ and the film thickness is determined from (18).

4.2. Weak saturation

When $\phi_\mathrm{e} = O(\mathrm{Pe}^{1/a})$ or smaller, the time scale on which the surface of the film approaches equilibrium saturation becomes smaller than or commensurate with the time that is required for the saturation front to reach the substrate. The expansion of the film occurs before the solvent fraction reaches a quasi-steady state and thus the evolution of the film thickness deviates from that predicted by (19), as shown in Figure S8. We leave a detailed analysis of this saturation stage as an area of future work.

5. Model validation with experiments

Film drying and sorption experiments were carried out as a means of (i) verifying that the mathematical model presented in Section 2 is able to accurately describe these processes and (ii) illustrating how the asymptotic solutions can be used to extract key physical parameters of the system. The experiments are based on ternary solutions consisting of aluminium chlorohydrate (ACH; 50 wt% hydrated dialuminum chloride pentahydroxide aqueous solution, Summit Research Laboratories Inc.), glycerol (Sigma-Aldrich), and deionised water (obtained from a Milli-Q source), which act as model systems for an important class of personal care products, namely anti-perspirants [14]. Typical drying rates for these systems are relatively slow, of the order of 1 μm·min^{-1}, commensurate with a range of paint-drying, dip-coating, and other drying processes [64, 65, 66, 67]. For drying processes of considerably higher rates ($\sim$100 μm·min^{-1}), a nonlinear expression for the solvent flux J might be required, as discussed in Section S2 of the Supplementary Material.

At atmospheric pressures and temperatures below 40 °C, only water evaporates ("solvent") while both ACH and glycerol remain in the solution or film ("solutes") [14]. Glycerol acts as a "humectant" and modulates both drying and sorption/desorption kinetics, as well as the thermodynamics of the system. Under certain conditions [11, 14], a transient skin is formed upon drying. When applying the model (12) to this system, the mixture is effectively "coarse-grained" such that the two solutes, glycerol and ACH, are treated as a single non-volatile component with volume fraction $1 - \phi$. The ternary mixture thus becomes "pseudo-binary". Importantly, however, the model parameters, namely the diffusion and mass transfer coefficients, are dependent on the ACH-glycerol ratio, enabling the accurate parameterisation of the ternary system.

Solutions were prepared with a fixed ACH mass fraction of 0.15 and varying glycerol mass fractions ranging from 0 up to 0.15. After preparation, the solutions were left to homogenise and reach equilibrium over a time span of two hours. Thin films of height 130 ± 10 μm were then prepared by depositing 10 μl of solution onto a balance pan using a pipette (Eppendorf). Dynamic vapour sorption (DVS-Advantage, Surface Measurement Systems Inc.) was used to monitor the change in mass of the film during the evaporation/absorption processes with a resolution of ± 10 μg. The measurements of the film mass were then converted into film thickness by assuming that the cross-sectional area of the film remained constant during each experiment. The relative humidity (RH) of the atmosphere was controlled by pumping a mixture of air and water vapour into the drying chamber at a standard total gas flow rate of 200 sccm, which otherwise had little influence on the evaporation/absorption processes.

The equipment was programmed to carry out the experiments as follows. First, the initial films were dried for a period of five hours at 0% RH. During this time, the film mass reached a steady state, signifying the end of the drying process. Film sorption was then initiated by increasing the RH to 20% and maintaining this value for 200–400 minutes. In the case of a 0% glycerol mixture, a sequence of alternating absorption/evaporation cycles followed the initial drying period whereby the RH of each absorption cycle was increased from 0% to 80% in 20% increments and held for 480 minutes. After each absorption cycle, the saturated film was dried at 0% RH for 480 minutes.

Due to the presence of ACH and glycerol in the films, it was possible for the total water loss in the drying experiments to exceed the initial amount of deionised water that was added to the mixtures. This "enhanced drying" is explained by the presence of water in the initial ACH complexes. During drying, the water in the ACH com-

plexes is exchanged with glycerol and the excess is free to evaporate from the film [14]. Accounting for water in the ACH complexes is possible by a judicious choice of the parameter ϕ_i, which represents the initial fraction of water in the film. In practice, ϕ_i is calculated in the drying experiments using measurements of the equilibrium film thickness and (13) under the assumption that $\phi_\mathrm{e} = 0$.

5.1. Drying experiments

Experimental data from drying experiments using films consisting of 0% and 15% glycerol are presented in Figure 6 (a). As predicted from the analysis of film drying in Section 3.1, the evaporation process can be decomposed into multiple stages. First, there is an initial period whereby a significant fraction of water is shed from the layer and the film thins at a rate that is approximately constant [stages (i)–(ii)]. The rate of thinning then decreases [stages (iii)–(iv)] and subsequent changes in the film thickness are small.

Values for the physical parameters associated with the films can be estimated by fitting the non-dimensional model (12) to the experimental data. As previously mentioned, we take $\phi_\mathrm{e} = 0$ and calculate ϕ_i from the equilibrium film thickness using (13). Thus, the non-dimensional model depends on four unknown parameters: a, Pe, δ, and the evaporative time scale $\tau_\mathrm{evap} = h_\mathrm{i}/k$. The latter three of these act as proxies for the physical parameters D_0, D_∞, and k, respectively. Three of these four parameters can be easily determined by fitting the asymptotic solutions of the drying problem to the experimental data.

A visual guide of the fitting procedure is given in Figure 6 (b). First, a value for the mass transfer coefficient k is determined by fitting the asymptotic solution for the film thickness in stage (ii), given by the dimensional version of (14), to the constant-rate period of the drying curve, which we identify as the initial portion of the curve with negative curvature. Eventually, the asymptotic solution of stage (ii) begins to deviate from the experimental data, which marks the transition into the third drying stage. From the analysis of Section 3.1.3, this transition is expected to occur when the film thickness is of order $h \sim h_\infty(1 + \mathrm{Pe}^{1/a})$; see (15). Therefore, a value of $\mathrm{Pe}^{1/a} = (kh_\mathrm{i}/D_0)^{1/a}$ can be determined by calculating $(h - h_\infty)/h_\infty$ at the point at which the asymptotic solution in stage (ii) begins to depart from the experimental data. In Figure 6 (b), this departure can be seen to begin when $(h - h_\infty)/h_\mathrm{i} \simeq 10^{-2}$. The dry diffusivity D_∞ can be calculated using the asymptotic thinning rate of stage (iv); in dimensional terms, this is given by

$$\frac{\mathrm{d}}{\mathrm{d}t}\left[\log\left((h - h_\infty)/h_\mathrm{i}\right)\right] = -\lambda_0^2(1 - \phi_\mathrm{i})^{-2}(D_\infty/h_\mathrm{i}^2), \quad (22)$$

where λ_0 solves $\lambda_0 \tan(\lambda_0) = (1 - \phi_\mathrm{i})(kh_\mathrm{i}/D_\infty)$. However, if $(1 - \phi_\mathrm{i})(kh_\mathrm{i}/D_\infty) \gg 1$, which is expected when there is a significant reduction in the thinning rate due to skin formation, then $\lambda_0 \sim \pi/2$. Therefore, a value of D_∞ can be straightforwardly estimated using (22) after the rate on the left-hand side has been calculated from the experimental data and λ_0 is approximated by $\pi/2$.

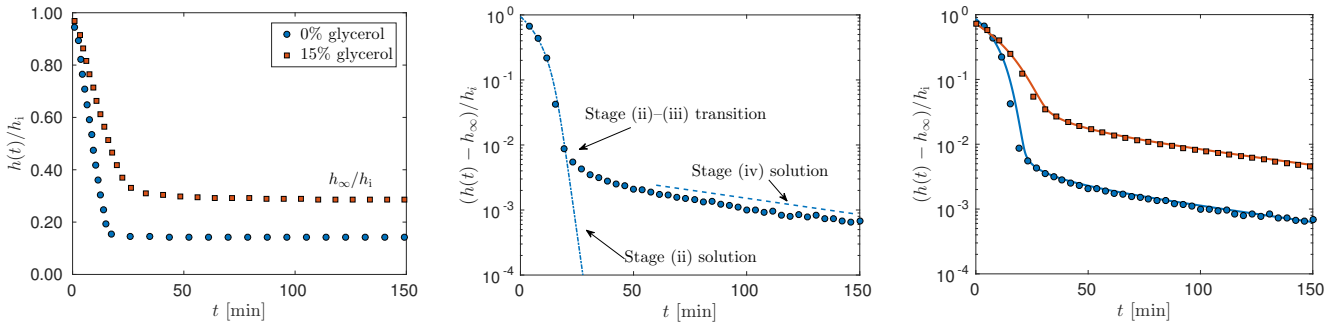
This fitting methodology determines three of the four model parameters. The final step in the fitting is to isolate the values of a and D_0. To do this, numerical solutions of the full non-dimensional model (12) are fit to the experimental data using Pe as the single fitting parameter. Knowing Pe, the values of a and δ can subsequently be determined.

The solid lines in Figure 6 (c) correspond to numerical simulations of the model using parameters obtained by our fitting procedure. The model is able to capture the experimental data with a remarkable degree of accuracy. Model parameters for the film with 0% glycerol were found to be $\phi_\mathrm{i} = 0.86$, $\tau_\mathrm{evap} = 14$ min, $a = 3.8$, $\mathrm{Pe} = 1.0 \cdot 10^{-4}$, and $\delta = 1.3{\cdot}10^{-7}$. In terms of dimensional quantities based on an initial film thickness of $h_\mathrm{i} = 130$ μm, we find that $k = 9.2 \cdot 10^{-6}$ m·min^{-1}, $D_0 = 1.2 \cdot 10^{-5}$ m^2·min^{-1}, and $D_\infty = 1.6 \cdot 10^{-12}$ m^2·min^{-1} For the 15% glycerol film, the model parameters are $\phi_\mathrm{i} = 0.72$, $\tau_\mathrm{evap} = 20$ min, $a = 4.0$, $\mathrm{Pe} = 7.0 \cdot 10^{-4}$, and $\delta = 5.1 \cdot 10^{-6}$, which lead to values of $k = 6.5 \cdot 10^{-6}$ m·min^{-1}, $D_0 = 1.2 \cdot 10^{-6}$ m^2·min^{-1}, and $D_\infty = 6.2 \cdot 10^{-12}$ m^2·min^{-1}. The higher value of D_∞ in the latter case is expected due to the plasticisation of the film by the addition of glycerol, suppressing its glass transition at room temperature, and the trivial reduction of the ACH phase volume.

Using the values of the physical parameters obtained for the 0% and 15% glycerol mixtures, it is now possible to make quantitative predictions about the drying dynamics that occur in films with different initial compositions and thicknesses. For instance, Figure 7 (a) shows a contour plot of the drying curves for arbitrary glycerol fractions between 0–15% that have been computed by simulating the model with parameter values obtained by interpolation. From this data, it is possible to predict, for a given composition, the time that is required for 99% of the solvent to be removed from the film, which is shown as the dashed curve in Figure 7 (a). Figure 7 (b) illustrates how the drying curves depend on the initial height of the film when the initial glycerol fraction is held at 15%. The dashed-dot line shows the time t_{95} that is required for 95% of the solvent to evaporate from the film. The linear relationship between t_{95} and h_i arises from the fact that, up to this point, the films are in stage (i)–(ii) of the drying process and thus the time scale is set by that of evaporation, h_i/k. These figures illustrate how the model can provide a wealth of quantitative insight into film drying over a wide range of conditions from only a small amount of experimental data.

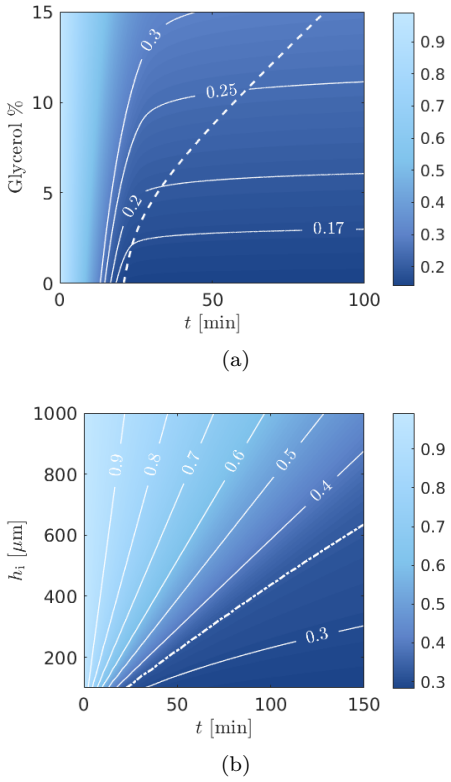
5.2. Sorption experiments

Figure 8 (a) presents the data from sorption experiments using a 0% glycerol mixture at different values of RH. As the RH is increased, the film is able to absorb more water from the surrounding atmosphere and thus there is a corresponding increase in the equilibrium film



(a) Raw data (b) Asymptotics (c) Model

Figure 6: (Color online) Drying of ternary ACH-glycerol-water mixtures in 0% relative humidity. (a) Raw experimental data of the film thickness as a function of time. (b) A visual guide to fitting the asymptotic solutions of the drying problem to experimental data. The time scale of evaporation, h_i/k, can be determined by fitting the quasi-steady solution in stage (ii), given by (14), to the constant-rate period of the drying curve. The point at which the quasi-steady solution departs from the data can be used to infer a value of $\mathrm{Pe}^{1/a}$. The asymptotic thinning rate predicted from the solution in stage (iv), given by (16), can be used to calculate the dry diffusivity D_∞. (c) Model fits (lines) to experimental data (symbols) of 0% (circles) and 15% (squares) glycerol mixtures.



(a) (b)

Figure 7: (Color online) Predictions of the evolution of the (normalised) film thickness $h(t)/h_\mathrm{i}$ with time for (a) various initial glycerol compositions and fixed initial film thickness (130 μm), and (b) at fixed initial glycerol concentration (15%) and various film thicknesses, up to 1000 μm. In panel (a) the dashed line corresponds to the time required for 99% of the solvent (water) to evaporate. In panel (b) the dashed-dot line represents the time needed for 95% of the solvent (water) to evaporate.

thickness. Assuming that the films are dry at the start of each absorption cycle, corresponding to $\phi_\mathrm{i} = 0$, the equilibrium water fraction ϕ_e can be obtained via (13) using the final height of the film. We find that $\phi_\mathrm{e} = 0.070$, 0.14, 0.22, and 0.38 when the RH is set to 20%, 40%, 60%, and 80%, respectively. Motivated by the results of analysing the sorption problem in Section 4.1, we attempted to fit the experimental data to the asymptotic solution for the film thickness (19). The only free parameter in the fitting is the time scale of absorption $\tau_\mathrm{abs} = h_\mathrm{i}/k$, which was found to be 4.8, 3.2, 2.8, and 4.4 min for the absorption cycles at 20%, 40%, 60%, and 80% RH, respectively. The results from the fits are shown as lines in Figure 8 (a); the agreement between theory and experimental is excellent.

In the final set of sorption experiments, the RH was fixed to 20% and the role of the glycerol fraction was investigated. The data from these experiments is tabulated in Table S1. The relative increase in the film thickness, as measured by the value of $h_\infty/h_\mathrm{i} - 1$, was found to be small, suggesting that only a small fraction of water is absorbed in these low-RH conditions. Calculating the equilibrium fraction according to (13) revealed that ϕ_e was indeed small for all of the mixtures that were considered. The analysis of the sorption problem suggests that any experimental data associated with small equilibrium solvent fractions should collapse onto a master curve given by (21). Thus, we attempted to fit the experimental data of the film thickness as a function of time, shown as symbols in Figure 8 (b), to the exponential function given by (20) to determine the time scale of absorption τ_abs. When carrying out the fitting, an approximate value for ϕ_e, given by $\phi_\mathrm{e} \simeq h_\infty/h_\mathrm{i} - 1$, was used in order to be consistent with the small-ϕ_e approximation. The experimental data obtained from films with 0%–10% glycerol fits nicely onto the master curve, shown as a solid black line. Interestingly, the data from the film with 15% glycerol seems to slightly deviate from the master curve, possibly indicating that this

system lies outside of the strong-saturation limit that was analysed in Section 4.1. Resolving this discrepancy will be an area of future work.

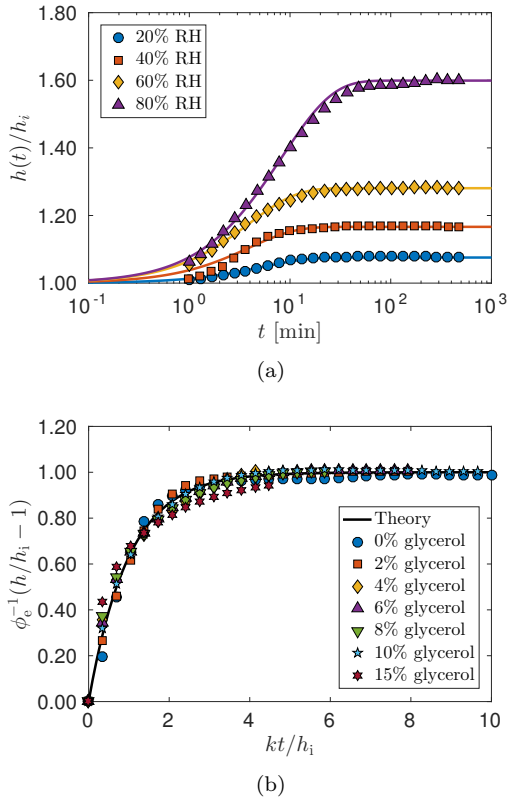


Figure 8: (Color online) Sorption experiments using ternary ACH-glycerol-water mixtures. (a) The effect of RH on the saturation of 0% glycerol mixtures that begin from the dry state, characterised by $\phi_i = 0$. Symbols denote experimental data and the solid lines correspond to the quasi-steady solution given by (19). (b) Sorption experiments carried out at 20% RH. The experimental data (symbols) can be collapsed onto a master curve (solid line) given by (21) due to the smallness of the equilibrium volume fraction ϕ_e at 20% RH; parameters from the fit are given in Table S1.

6. Conclusion

We have presented a minimal model of solvent evaporation and absorption in thin films, based on physical parameters that are limited in number and relatively easy to determine, which can be used as a predictive tool. In contrast to explicit models that consider detailed physical-chemical processes [50, 51, 52], the minimal model is analytically tractable. Thus, an asymptotic study of the model was carried out, which yielded novel analytical expressions that can be used to extract parameter values from experimental data. In addition, the asymptotic analysis revealed key insights into the dynamics that can occur during the drying and sorption processes. In the case of evaporation, a state diagram can be constructed which outlines the stages that occur along the drying pathway. Importantly, this diagram can also be used to predict the experimental conditions that will lead to the formation of a solute-rich skin near the evaporating surface. Such skins play important roles in, e.g., paints [35] and spin-cast polymer films [33]. Having predictive control over the physical characteristics of these skins can, therefore, open innovative pathways for surface patterning and the fabrication of advanced functional surfaces [9].

A comparison of the theoretical results with data produced from dynamic vapour sorption experiments showed that the model is able to accurately capture key features of evaporation and absorption. In the case of solvent absorption, the kinetics were entirely set by the mass transfer coefficient k and the film thickness could be described by a single implicit function. The relatively small time scale on which diffusion plays a leading role in the sorption problem meant that diffusive effects could not be detected in the measurements of the film thickness, the latter of which evolves on a much larger time scale. This fact had important practical ramifications, as the sorption experiments were unable to provide information about the diffusivity of solvent within the film. The situation is slightly different in the drying problem because the eventual formation of a skin reduces the rate of thinning enough for the diffusion-limited stage to be detectable in measurements of the film thickness. In situations where no skin occurs, the drying problem becomes similar to the sorption problem in the sense that the rate of thinning is solely driven by evaporation and hence set by the mass transfer coefficient.

In deriving the minimal model, several simplifying assumptions were imposed in order to retain the analytical tractability of the governing equations. If these assumptions cease to be valid, then the model may need to be extended. For example, evaporative cooling can influence the drying dynamics through changes in the diffusivity, which often has an Arrhenius-like temperature dependence, or via the mass transfer coefficient appearing in the evaporative flux. The effects of evaporative cooling may only influence the early stages of drying, however, due to the fact that the thermal diffusivity is often much larger than the mass diffusivity [68]; therefore, the film reaches thermal equilibrium before it thins by an appreciable amount. Due to the simplicity and generality of the model, incorporating additional physics and using alternative forms of the phenomenological laws, e.g., for the diffusivity, is a straightforward task.

Perhaps the most significant modelling assumption is the treatment of the system as one dimensional. When this assumption is combined with that of a flat surface, our model effectively only considers films with constant surface area. Such films are rarely encountered in practice and, therefore, the predictions from a one-dimensional model could deviate slightly from experimental data due to geometric effects associated with the change in surface area. Extending the model to multiple spatial dimensions is certainly possible [63], although this can come with a marked increase in complexity as one begins to account for contact line motion and other hydrodynamic effects

[69]. However, the excellent agreement between our theoretical and experimental results, the latter of which involve films with pinned contact lines and a height-to-width ratio of roughly 1:100, suggests that our one-dimensional model can capture the key features with sufficient accuracy to function as a useful predictive tool of solvent evaporation and absorption in thin films.

Acknowledgements

We acknowledge the financial support from the Engineering and Physical Sciences Research Council (EPSRC) [grant numbers EP/K503733/1, EP/L020564/1], and the Royal Society (UK). Data is available on request: please contact polymer-microfluidics@imperial.ac.uk.

[1] C. Park, J. Yoon, E. L. Thomas, Enabling nanotechnology with self assembled block copolymer patterns, Polymer 44 (22) (2003) 6725–6760.

[2] S. Walheim, E. Schäffer, J. Mlynek, U. Steiner, Nanophase-separated polymer films as high-performance antireflection coatings, Science 283 (5401) (1999) 520–522.

[3] B.-J. de Gans, P. C. Duineveld, U. S. Schubert, Inkjet printing of polymers: state of the art and future developments, Adv. Mater. 16 (3) (2004) 203–213.

[4] B. Li, Y.-P. Cao, X.-Q. Feng, H. Gao, Mechanics of morphological instabilities and surface wrinkling in soft materials: a review, Soft Matter 8 (21) (2012) 5728–5745.

[5] W. Han, Z. Lin, Learning from "coffee rings": Ordered structures enabled by controlled evaporative self-assembly, Angew. Chem. Int. Edit. 51 (7) (2012) 1534–1546.

[6] A. Georgiadis, A. F. Routh, M. W. Murray, J. L. Keddie, Bespoke periodic topography in hard polymer films by infrared radiation-assisted evaporative lithography, Soft Matter 7 (23) (2011) 11098–11102.

[7] D. J. Harris, H. Hu, J. C. Conrad, J. A. Lewis, Patterning colloidal films via evaporative lithography, Phys. Rev. Lett. 98 (14) (2007) 148301.

[8] C. Parneix, P. Vandoolaeghe, V. S. Nikolayev, D. Quéré, J. Li, B. Cabane, Dips and rims in dried colloidal films, Phys. Rev. Lett. 105 (26) (2010) 266103.

[9] T. P. Russell, Surface-responsive materials, Science 297 (5583) (2002) 964–967.

[10] K. I. Dragnevski, A. F. Routh, M. W. Murray, A. M. Donald, Cracking of drying latex films: an ESEM experiment, Langmuir 26 (11) (2010) 7747–7751.

[11] G. L. Ferretti, M. Nania, O. K. Matar, J. T. Cabral, Wrinkling measurement of the mechanical properties of drying salt thin films, Langmuir 32 (9) (2016) 2199–2207.

[12] D. Y. Arifin, L. Y. Lee, C.-H. Wang, Mathematical modeling and simulation of drug release from microspheres: Implications to drug delivery systems, Adv. Drug Deliver. Rev. 58 (12) (2006) 1274–1325.

[13] J.-W. Rhim, Physical and mechanical properties of water resistant sodium alginate films, Lebensm. Wiss. Technol. 37 (3) (2004) 323–330.

[14] G. L. Ferretti, J. T. Cabral, Phase behaviour and non-monotonic film drying kinetics of aluminium chlorohydrate-glycerol-water ternary solutions, J. Colloid Interf. Sci. 481 (2016) 263–270.

[15] A. F. Routh, Drying of thin colloidal films, Rep. Prog. Phys. 76 (4) (2013) 046603.

[16] S. T. Eckersley, A. Rudin, Drying behavior of acrylic latexes, Prog. Org. Coat. 23 (4) (1994) 387–402.

[17] K. E. Davis, W. B. Russel, An asymptotic description of transient settling and ultrafiltration of colloidal dispersions, Phys. Fluids A-Fluid 1 (1) (1989) 82–100.

[18] T. Narita, P. Hebraud, F. Lequeux, Effects of the rate of evaporation and film thickness on nonuniform drying of film-forming concentrated colloidal suspensions, Eur. Phys. J. E 17 (1) (2005) 69–76.

[19] T. Okuzono, K. Ozawa, M. Doi, Simple model of skin formation caused by solvent evaporation in polymer solutions, Phys. Rev. Lett. 97 (13) (2006) 136103.

[20] A. F. Routh, W. B. Zimmerman, Distribution of particles during solvent evaporation from films, Chem. Eng. Sci. 59 (14) (2004) 2961–2968.

[21] P.-G. de Gennes, Solvent evaporation of spin cast films: "crust" effects, Eur. Phys. J. E 7 (1) (2002) 31–34.

[22] L. Pauchard, C. Allain, Buckling instability induced by polymer solution drying, Eurphys. Lett. 62 (6) (2003) 897.

[23] S. Alsoy, J. L. Duda, Modeling of multilayer drying of polymer films, J. Polym. Sci. Pol. Phys. 37 (14) (1999) 1665–1675.

[24] C. Peishi, D. C. T. Pei, A mathematical model of drying processes, Int. J. Heat Mass Trans. 32 (2) (1989) 297–310.

[25] P. E. Price, R. A. Cairncross, Optimization of single-zone drying of polymer solution coatings using mathematical modeling, J. Appl. Polym. Sci. 78 (1) (2000) 149–165.

[26] R. V. Craster, O. K. Matar, Dynamics and stability of thin liquid films, Rev. Mod. Phys. 81 (3) (2009) 1131.

[27] A. Oron, S. H. Davis, S. G. Bankoff, Long-scale evolution of thin liquid films, Rev. Mod. Phys. 69 (3) (1997) 931.

[28] R. D. Deegan, Pattern formation in drying drops, Phys. Rev. E 61 (1) (2000) 475.

[29] R. D. Deegan, O. Bakajin, T. F. Dupont, G. Huber, S. R. Nagel, T. A. Witten, Capillary flow as the cause of ring stains from dried liquid drops, Nature 389 (6653) (1997) 827–829.

[30] R. D. Deegan, O. Bakajin, T. F. Dupont, G. Huber, S. R. Nagel, T. A. Witten, Contact line deposits in an evaporating drop, Phys. Rev. E 62 (1) (2000) 756.

[31] M. R. E. Warner, R. V. Craster, O. K. Matar, Surface patterning via evaporation of ultrathin films containing nanoparticles, J. Colloid Interf. Sci. 267 (1) (2003) 92–110.

[32] M. G. Hennessy, C. J. W. Breward, C. P. Please, A two-phase model for evaporating solvent-polymer mixtures, SIAM J. Appl. Math. 76 (4) (2016) 1711–1736.

[33] A. Münch, C. P. Please, B. Wagner, Spin coating of an evaporating polymer solution, Phys. Fluids 23 (10) (2011) 102101.

[34] M. H. Eres, D. E. Weidner, L. W. Schwartz, Three-dimensional direct numerical simulation of surface-tension-gradient effects on the leveling of an evaporating multicomponent fluid, Langmuir 15 (5) (1999) 1859–1871.

[35] P. L. Evans, L. W. Schwartz, R. V. Roy, A mathematical model for crater defect formation in a drying paint layer, J. Colloid Interf. Sci. 227 (1) (2000) 191–205.

[36] M. G. Hennessy, A. Münch, A multiple-scale analysis of evaporation induced Marangoni convection, SIAM J. Appl. Math. 73 (2) (2013) 974–1001.

[37] M. G. Hennessy, A. Münch, Dynamics of a slowly evaporating solvent-polymer mixture with a deformable upper surface, IMA J. Appl. Math. 79 (4) (2014) 681–720.

[38] S. D. Howison, J. A. Moriarty, J. R. Ockendon, E. L. Terrill, S. K. Wilson, A mathematical model for drying paint layers, J. Eng. Math. 32 (4) (1997) 377–394.

[39] T. Alfrey, E. F. Gurnee, W. G. Lloyd, Diffusion in glassy polymers, in: J. Polym. Sci. Pol. Phys., Vol. 12, Wiley Online Library, 1966, pp. 249–261.

[40] M. Doi, Gel dynamics, J. Phys. Soc. Jpn. 78 (5) (2009) 052001.

[41] W. Hong, X. Zhao, J. Zhou, Z. Suo, A theory of coupled diffusion and large deformation in polymeric gels, J. Mech. Phys. Solids 56 (5) (2008) 1779–1793.

[42] M. Quesada-Pérez, J. A. Maroto-Centeno, J. Forcada, R. Hidalgo-Alvarez, Gel swelling theories: the classical formalism and recent approaches, Soft Matter 7 (22) (2011) 10536–10547.

[43] D. S. Cohen, A. B. White, Jr, Sharp fronts due to diffusion and viscoelastic relaxation in polymers, SIAM J. Appl. Math. 51 (2) (1991) 472–483.

[44] C.-Y. Hui, K.-C. Wu, R. C. Lasky, E. J. Kramer, Case-II diffusion in polymers. II. Steady-state front motion, J. Appl. Phys. 61 (11) (1987) 5137–5149.
[45] G. Rossi, P. A. Pincus, P.-G. de Gennes, A phenomenological description of case-II diffusion in polymeric materials, Europhys. Lett. 32 (5) (1995) 391.
[46] N. L. Thomas, A. H. Windle, A theory of case II diffusion, Polymer 23 (4) (1982) 529–542.
[47] D. S. Cohen, T. Erneux, Free boundary problems in controlled release pharmaceuticals. I: Diffusion in glassy polymers, SIAM J. Appl. Math. 48 (6) (1988) 1451–1465.
[48] S. L. Mitchell, S. B. G. O'Brien, Asymptotic, numerical and approximate techniques for a free boundary problem arising in the diffusion of glassy polymers, Appl. Math. Comput. 219 (1) (2012) 376–388.
[49] S. L. Mitchell, S. B. G. O'Brien, Asymptotic and numerical solutions of a free boundary problem for the sorption of a finite amount of solvent into a glassy polymer, SIAM J. Appl. Math. 74 (3) (2014) 697–723.
[50] P. E. Price, S. Wang, I. Hadj Romdhane, Extracting effective diffusion parameters from drying experiments, AIChE J. 43 (8) (1997) 1925–1934.
[51] M. Vinjamur, R. A. Cairncross, Non-fickian nonisothermal model for drying of polymer coatings, AIChE J. 48 (11) (2002) 2444–2458.
[52] M. Vinjamur, R. A. Cairncross, Experimental investigations of trapping skinning, J. Appl. Polym. Sci. 83 (10) (2002) 2269–2273.
[53] I. Hadj Romdhane, R. P. Danner, J. L. Duda, Influence of the glass transition on solute diffusion in polymers by inverse gas chromatography, Ind. Eng. Chem. Res. 34 (8) (1995) 2833–2840.
[54] Z. Gu, P. Alexandridis, Drying of films formed by ordered poly (ethylene oxide)-poly (propylene oxide) block copolymer gels, Langmuir 21 (5) (2005) 1806–1817.
[55] L. Ion, J. M. Vergnaud, Process of drying a polymeric paint by diffusion-evaporation and shrinkage. determination of the concentration-dependent diffusivity, Polymer testing 14 (5) (1995) 479–487.
[56] J. S. Vrentas, J. L. Duda, Diffusion in polymer-solvent systems. I. Reexamination of the free-volume theory, J. Polym. Sci. Pol. Phys. 15 (3) (1977) 403–416.
[57] I. Hadj Romdhane, P. E. Price, C. A. Miller, P. T. Benson, S. Wang, Drying of glassy polymer films, Ind. Eng. Chem. Res. 40 (14) (2001) 3065–3075.
[58] T. Okuzono, M. Doi, Effects of elasticity on drying processes of polymer solutions, Phys. Rev. E 77 (3) (2008) 030501.
[59] G. D. Verros, S. Papahristou, J. Prinos, N. A. Malamataris, Computer-aided estimation of acetone, methyl acetate, and chloroform diffusion coefficients in poly (vinyl acetate), Chem. Eng. Comm. 190 (3) (2003) 334–359.
[60] V. Sharma, L. Song, R. L. Jones, M. S. Barrow, P. R. Williams, M. Srinivasarao, Effect of solvent choice on breath-figure-templated assembly of "holey" polymer films, Europhys. Lett. 91 (3) (2010) 38001.
[61] C.-C. Chang, C.-L. Pai, W.-C. Chen, S. A. Jenekhe, Spin coating of conjugated polymers for electronic and optoelectronic applications, Thin Solid Films 479 (1) (2005) 254–260.
[62] R. K. Arya, M. Vinjamur, Near-optimization of operating conditions and residence times in multizone dryers for polymer coatings, Ind. Eng. Chem. Res. 48 (23) (2009) 10504–10514.
[63] J. S. Vrentas, C. M. Vrentas, Drying of solvent-coated polymer films, J. Polym. Sci. Poly. Phys 32 (1) (1994) 187–194.
[64] W. S. Overdiep, The levelling of paints, Prog. Org. Coat. 14 (2) (1986) 159–175.
[65] H. Bodiguel, F. Doumenc, B. Guerrier, Stick- slip patterning at low capillary numbers for an evaporating colloidal suspension, Langmuir 26 (13) (2010) 10758–10763.
[66] M. Ghosh, F. Fan, K. J. Stebe, Spontaneous pattern formation by dip coating of colloidal suspensions on homogeneous surfaces, Langmuir 23 (4) (2007) 2180–2183.
[67] S. P. Paradiso, K. T. Delaney, C. J. García-Cervera, H. D. Ceniceros, G. H. Fredrickson, Block copolymer self assembly during rapid solvent evaporation: Insights into cylinder growth and stability, ACS Macro Letters 3 (1) (2013) 16–20.
[68] N. Bassou, Y. Rharbi, Role of Benard–Marangoni instabilities during solvent evaporation in polymer surface corrugations, Langmuir 25 (1) (2008) 624–632.
[69] G. Karapetsas, K. Chandra Sahu, O. K. Matar, Evaporation of sessile droplets laden with particles and insoluble surfactants, Langmuir 32 (27) (2016) 6871–6881.

Supplementary material

A minimal model for solvent evaporation and absorption in thin films

Matthew G. Hennessy*, Giulia L. Ferretti, João T. Cabral, Omar K. Matar*

S1 Graphical overview

Figure S1 provides a graphical overview of how the model can be applied to the problem of film drying. The same approach can be used to study the swelling of a film that occurs upon solvent absorption.

S2 Comparison of models for the solvent flux

The minimal model (12) is based on a simplified form of the solvent flux at the free surface given by

$$J_1(\phi) = k_1(\phi - \phi_\mathrm{e}), \tag{S1}$$

where k_1 is a mass transfer coefficient and ϕ_e is the equibrium solvent fraction. Generally, the solvent flux is expressed in terms of the difference in vapour pressures [5]. In the case of solvent-polymer mixtures [2, 4], the flux can be written as a nonlinear function of the solvent fraction,

$$J_2(\phi) = k_2 \left[\phi\, \mathrm{e}^{1-\phi+\chi(1-\phi)^2} - \phi_\mathrm{e}\, \mathrm{e}^{1-\phi_\mathrm{e}+\chi(1-\phi_\mathrm{e})^2}\right], \tag{S2}$$

where χ is the interaction parameter in the Flory–Huggins free energy and k_2 is another mass transfer coefficient. For $\phi \sim \phi_\mathrm{e}$, we find that $J_2(\phi) \sim k_2'(\phi - \phi_\mathrm{e})$, with k_2' representing a constant that depends on k_2 and ϕ_e. Therefore, the flux given by (S1) can be interpreted as the near-equilibrium limit of (S2). Moreover (S1) is expected to be a valid approximation of (S2) provided that $|\phi_\mathrm{i} - \phi_\mathrm{e}| \ll 1$, where ϕ_i is the initial solvent fraction. To explore the validity of this approximation when $|\phi_\mathrm{i} - \phi_\mathrm{e}| = O(1)$, numerical simulations of the dimensionless model (12) using a solvent flux given by (S2) have been carried out. The mass transfer coefficient k_2 in the nonlinear flux (S2) is chosen so that $J_1(\phi_\mathrm{i}) = J_2(\phi_\mathrm{i})$. This will ensure that the rates of change of film thickness are initially equal and that the same non-dimensionalisation can be applied when using the nonlinear flux.

Figure S2 (a) shows the evolution of the film thickness in the drying problem when $\phi_\mathrm{e} = 0$ and $\phi_\mathrm{i} = 0.85$. The other parameters are $\mathrm{Pe} = 10^{-2}$, $\delta = 10^{-5}$, $a = 3.0$, and $\chi = 0.40$. As the nonlinear flux (S2) is greater than the simplified linear flux (S1), the solutions begin to diverge during the the constant-rate period of drying, which is evaporation-limited and thus governed by the form of the evaporative flux. However, once the system enters the diffusion-limited falling-rate period of drying, which occurs when $t \sim 2$ in Figure S2 (a), the differences in the evaporative flux become insignificant and the solutions begin to converge. In this case, the nonlinear flux (S2) only leads to small quantitative changes in the drying curve.

The situation is slightly different in the sorption problem because the diffusion-limited regime is short-lived and thus the majority of the evolution is set by the kinetics of solvent absorption. As Figure S2 (b) shows, differences in the form of the flux can lead to significant quantitative changes in the film thickness, although the qualitative behaviour remains the same. The simulations in Figure S2 (b) are based on $\phi_\mathrm{i} = 0$, $\phi_\mathrm{e} = 0.70$, $\mathrm{Pe} = 10^{-4}$, $\delta = 10^{-5}$, $a = 2.0$, and $\chi = 0.40$. The nonlinear flux (S2) is smaller (in magnitude) than the simplified flux (S1), which causes the film to expand more slowly in this case.

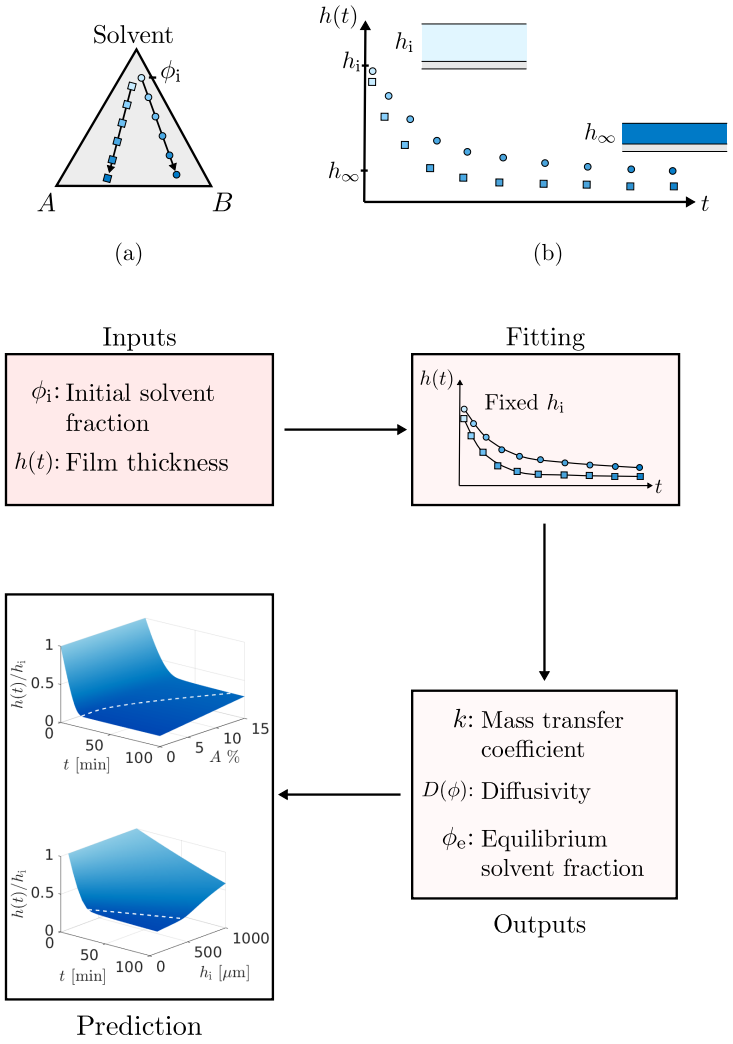
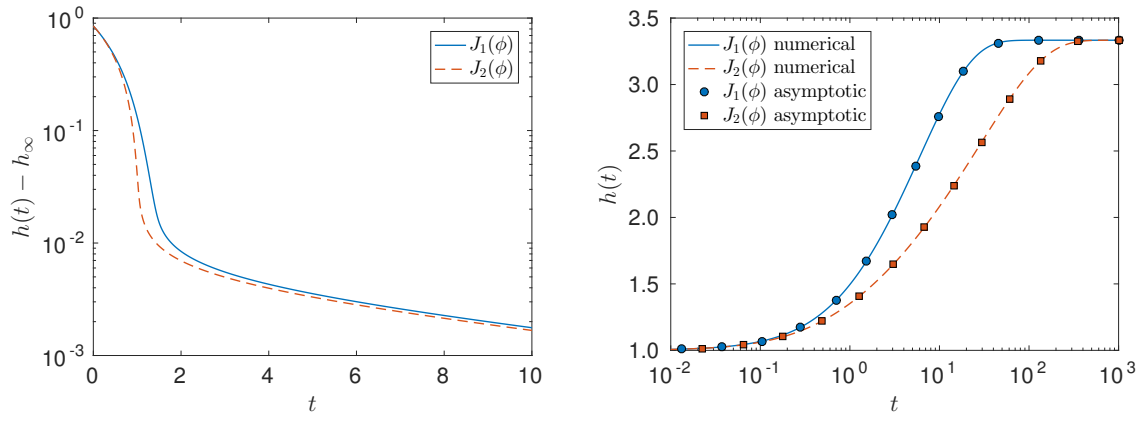


Figure S1: (Color online) An overview of a typical drying experiment and application of the model. (a) The drying of ternary mixtures consisting of two solutes, A and B, and a volatile solvent with distinct initial compositions will take place along different pathways in the phase diagram. (b) As these systems dry, the film thickness (or equivalently, the film mass) is measured as a function of time. (c) Using the initial solvent fraction ϕ_i and film thickness $h(t)$ as model inputs and fitting the solutions to experimental data, values for the mass transfer coefficient, k, and equilibrium solvent fraction, ϕ_e, as well as a functional form for the diffusivity, $D(\phi)$, can be obtained. Having determined all of the physical parameters, the model can then be used to predict how the drying process proceeds for different initial compositions (e.g., $A\%$), and film thicknesses (h_i).



(a) (b)

Figure S2: (Color online) Comparison of solvent evaporation and absorption using the simplified flux (S1) and the nonlinear flux (S2) in the dimensionless model (12). (a) Evolution of the film thickness in the drying problem. The model parameters are $\phi_\mathrm{i} = 0.85$, $\phi_\mathrm{e} = 0$, $\mathrm{Pe} = 10^{-2}$, $\delta = 10^{-5}$, $a = 3$, and $\chi = 0.4$. (b) Evolution of the film thickness in the sorption problem. Lines correspond to numerical simulations and symbols are asymptotic solutions. The model parameters are $\phi_\mathrm{i} = 0$, $\phi_\mathrm{e} = 0.7$, $\mathrm{Pe} = 10^{-4}$, $\delta = 10^{-5}$, $a = 2$, and $\chi = 0.4$.

The asymptotic analysis of the sorption problem with the nonlinear flux (S2) follows the same procedure detailed below in Section S5 for the case of the simplified flux (S1). Carrying out the asymptotic analysis with the nonlinear flux yields a simple (non-dimensional) differential equation for the film thickness given by

$$\frac{\mathrm{d}h}{\mathrm{d}t} = J_2\big(1 - (1-\phi_\mathrm{i})/h(t)\big) \tag{S3}$$

which must satisfy $h(0) = 1$. Figure S2 (b) shows that solutions of (S3) are excellent approximations to numerical solutions of the full nonlinear model (12). Furthermore, solving (S3) provides a straightforward way of fitting an extended model based on the nonlinear flux (S2) to experimental data.

S3 Details of the numerical method

In order to numerically implement the dimensionless model (12), we make the change of variable $\eta = z/h(t)$, which enables the moving domain $0 \leq z \leq h(t)$ to be transformed to a fixed domain $0 \leq \eta \leq 1$. The proceeding analysis, however, will be carried out using the dimensionless coordinate z. Linear finite elements are used to spatially discretise the diffusion equation (12a) in transformed coordinates. At each time step, we assume the film thickness is known and then update the solvent volume fraction using a semi-implicit method that treats the diffusive terms implicitly but the nonlinear terms (e.g., the diffusion coefficient) explicitly. Thus, updating the volume fraction requires solving a linear system of equations at each time step. Once a new volume fraction is computed, the film thickness is updated using an explicit time discretisation of (12d).

S4 Asymptotic analysis of solvent-rich film drying

The dynamics that occur in the four drying stages are now explored using matched asymptotic expansions and numerical simulations. For convenience, these stages are illustrated in Figure S3.

S4.1 Stage (i): Initial depletion

This stage is captured by writing $t = \varepsilon\hat{t}$, $\phi = \phi_\mathrm{i}(1 + \varepsilon\hat{\phi})$, and $h = 1 + \varepsilon\hat{h}$ in the dimensionless model (12), where the scaling for ϕ comes from balancing terms in the boundary condition at the film surface (12c).

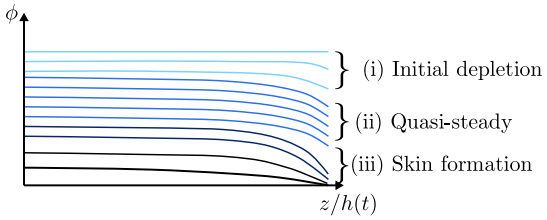


Figure S3: (Color online) A simplified schematic diagram of the key stages in solvent-rich film drying. There is a fourth stage (not shown), which is a continuation of the skin-formation stage and describes the removal of all remaining solvent from the film.

Assuming that the diffusivity does not change too rapidly and the condition $a\varepsilon|\hat{\phi}| \ll 1$ is satisfied, then we can naively take $\varepsilon \to 0$ to obtain the leading-order problem given by

$$\frac{\partial \hat{\phi}}{\partial \hat{t}} = \bar{D}(1)\frac{\partial^2 \hat{\phi}}{\partial z^2}, \tag{S4}$$

where the rescaled diffusivity $\bar{D}$ is defined as $\bar{D}(\bar{\phi}) = \bar{\phi}^a + \bar{\delta}$, with $\bar{\delta} = \delta\phi_{\mathrm{i}}^{-a}$, which is subject to the conditions

$$\frac{\partial \hat{\phi}}{\partial z} = 0, \qquad z = 0, \tag{S5a}$$

$$-\bar{D}(1)\frac{\partial \hat{\phi}}{\partial z} = 1 - \phi_{\mathrm{i}}, \quad z = 1, \tag{S5b}$$

$$\hat{\phi} = 0, \qquad \hat{t} = 0. \tag{S5c}$$

The leading-order solution for the film thickness is found to be

$$\hat{h}(\hat{t}) = -\phi_{\mathrm{i}}\hat{t}. \tag{S6}$$

The problem given by (S4)–(S5) can be solved using a Fourier series expansion and the early-time behaviour is readily deduced by seeking a similarity solution; for details, see Hennessy & Münch [3]. For our purposes it will suffice to consider the asymptotic behaviour for large $\hat{t}$. This can be obtained by first noting that

$$\int_0^1 \hat{\phi}(z,\hat{t})\,\mathrm{d}z = -(1-\phi_{\mathrm{i}})\hat{t}; \tag{S7}$$

this expression can be derived by integrating (S4) over the thickness of the film and applying the boundary and initial conditions in (S5). We now introduce an artificial small parameter $\alpha \ll 1$ and write $\hat{t} = \alpha^{-1}\check{t}$. From (S7) we must have that $\hat{\phi} \sim \alpha^{-1}$ if $\hat{t} \sim \alpha^{-1}$; thus, we write $\hat{\phi} = \alpha^{-1}\hat{\phi}_0 + \hat{\phi}_1 + O(\alpha)$. By solving the problem at each order of α we find that

$$\hat{\phi}(z,\hat{t}) \sim -(1-\phi_{\mathrm{i}})\hat{t} + \frac{(1-\phi_{\mathrm{i}})}{\bar{D}(1)}\left(\frac{1}{6} - \frac{z^2}{2}\right), \quad \hat{t} \gg 1. \tag{S8}$$

Therefore, the long-term solution in stage (i), written in terms of the original variables, is given by

$$\phi(z,t) \sim \phi_{\mathrm{i}} - (1-\phi_{\mathrm{i}})\phi_{\mathrm{i}}t + \frac{\mathrm{Pe}(1-\phi_{\mathrm{i}})\phi_{\mathrm{i}}}{D(\phi_{\mathrm{i}})}\left(\frac{1}{6} - \frac{z^2}{2}\right), \tag{S9a}$$

$$h(t) \sim 1 - \phi_{\mathrm{i}}t, \tag{S9b}$$

which is valid as $t \sim \varepsilon = \mathrm{Pe}\,\phi_{\mathrm{i}}^{-a} \ll 1$. The long-term solution (S9) will be used to match into the second stage.

S4.2 Stage (ii): Quasi-steady

This stage is captured by writing $\phi = \phi_\mathrm{i}\bar{\phi}$ and $h = \bar{h}$ in the dimensionless model given by (12a)–(12f). This leads to a diffusion equation of the form

$$\varepsilon\frac{\partial\bar{\phi}}{\partial t} = \frac{\partial}{\partial z}\left[\bar{D}(\bar{\phi})\frac{\partial\bar{\phi}}{\partial z}\right], \tag{S10a}$$

which has boundary conditions

$$\frac{\partial\bar{\phi}}{\partial z} = 0, \qquad z = 0, \tag{S10b}$$

$$-\bar{D}(\bar{\phi})\frac{\partial\bar{\phi}}{\partial z} = \varepsilon(1-\phi_\mathrm{i}\bar{\phi})\bar{\phi} \quad z = \bar{h}(t). \tag{S10c}$$

The film thins according to

$$\frac{\mathrm{d}\bar{h}}{\mathrm{d}t} = -\phi_\mathrm{i}\bar{\phi}(\bar{h}(t),t), \tag{S10d}$$

and the integral (12f) is given by

$$\phi_\mathrm{i}\int_0^{\bar{h}(t)}\bar{\phi}(z,t)\,\mathrm{d}z = \bar{h}(t) - 1 + \phi_\mathrm{i}. \tag{S10e}$$

Initial conditions are replaced by the requirement that the solution matches to (S9) as $t \sim 0$.

The governing equations (S10) are solved by seeking an asymptotic expansion of the form

$$\bar{\phi}(z,t) = \bar{\phi}_0 + \varepsilon\bar{\phi}_1 + O(\varepsilon^2), \tag{S11a}$$

$$\bar{h}(t) = \bar{h}_0 + \varepsilon\bar{h}_1 + O(\varepsilon^2), \tag{S11b}$$

and making the crucial assumption that $\bar{\phi} \gg \varepsilon^{1/a}$. If this is the case, then the leading-order (in ε) contributions of (S10a)–(S10c) imply that $\bar{\phi}_0$ is only a function of time. The leading-order part of (S10e) can then be used to relate the solvent fraction $\bar{\phi}_0$ to the film thickness $\bar{h}_0$; in particular,

$$\bar{\phi}_0(t) = \frac{\bar{h}_0(t) - 1 + \phi_\mathrm{i}}{\phi_\mathrm{i}\bar{h}_0(t)}. \tag{S12}$$

Inserting (S12) into the leading-order part of the thin-film equation (S10d) gives an initial value problem for the film thickness,

$$\frac{\mathrm{d}\bar{h}_0}{\mathrm{d}t} = -1 + \frac{(1-\phi_\mathrm{i})}{\bar{h}_0}, \tag{S13}$$

which has the matching condition $\bar{h}_0 = 1$ as $t = 0$, as dictated by (S9b), which also yields $\bar{\phi}_0(0) = 1$. An implicit solution for $\bar{h}_0$ can be obtained and written as

$$\bar{h}_0(t) + (1-\phi_\mathrm{i})\log\left[\frac{\bar{h}_0(t) - 1 + \phi_\mathrm{i}}{\phi_\mathrm{i}}\right] + t = 1. \tag{S14}$$

To better understand the onset of solute-rich skins, we must proceed to the $O(\varepsilon)$ problem because the leading-order solution for the solvent fraction given by (S12) is constant in space and thus does not provide any information about the development of concentration gradients. The $O(\varepsilon)$ solution for the solvent fraction can be written as

$$\bar{\phi}_1(z,t) = -\frac{(1-\phi_\mathrm{i})(\bar{h}_0 - 1 + \phi_\mathrm{i})}{2\phi_\mathrm{i}\bar{h}_0^3\bar{D}(\bar{\phi}_0)}\,z^2 + \bar{\phi}_1(0,t). \tag{S15}$$

Matching to the solution in stage (i), i.e., (S9a), yields $\bar{\phi}_1(0,0) = (1-\phi_\mathrm{i})/(6\bar{D}(1))$. A coupled system of differential equations that governs the undetermined function $\bar{\phi}_1(0,t)$ and the correction to the film

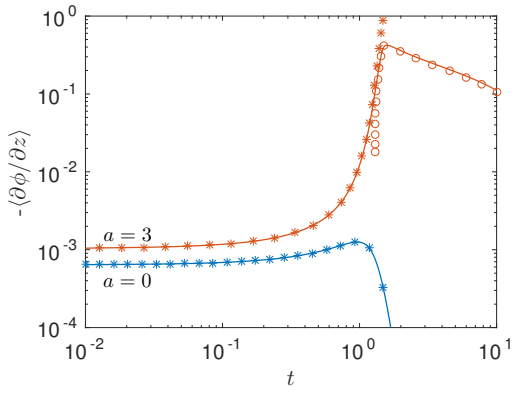


Figure S4: (Color online) Evolution of the average concentration gradient across the film defined by (S16) during film drying. Lines correspond to numerical simulations. Stars and circles correspond to the asymptotic solution in stages (ii) and (iii)–(iv), respectively. Parameters are $\phi_\mathrm{i} = 0.85$, $\mathrm{Pe} = 10^{-2}$, $\delta = 10^{-5}$, and $\phi_\mathrm{e} = 0$.

thickness $\bar{h}_1(t)$ can be derived from the $O(\varepsilon)$ contributions to the integral (S10e) and the equation for the film thickness (S10d). However, we do not pursue the solution to this problem here.

Using the $O(\varepsilon)$ solution for the solvent fraction (S15), we examine the average concentration gradient defined by

$$\left\langle \frac{\partial \phi}{\partial z} \right\rangle = \frac{\phi(h(t),t) - \phi(0,t)}{h(t)}. \tag{S16}$$

By inserting (S15) into (S16), we see that the undetermined function $\bar{\phi}_1(0,t)$ drops out and the average concentration gradient in the second time stage can be written as

$$\left\langle \frac{\partial \bar{\phi}}{\partial z} \right\rangle = -\frac{\varepsilon(1-\phi_\mathrm{i}\bar{\phi}_0)\bar{\phi}_0}{2\bar{D}(\bar{\phi}_0)} + O(\varepsilon^2). \tag{S17}$$

Upon neglecting the small $\bar{\delta}$ contribution to the diffusivity $\bar{D}$, the gradient in (S16) is approximately given by $\langle \partial\bar{\phi}/\partial z \rangle \sim -\varepsilon\bar{\phi}_0^{1-a}$, which can be interpreted as the ratio of solvent left in the film, $\bar{\phi}_0$, to the diffusivity $\bar{\phi}_0^a$. On one hand, the gradient tends to decrease as solvent is removed from the film, while on the other hand, it tends to increase as the diffusivity decreases during the drying process. The overall change in the gradient will depend on the rates at which these two quantities tend to zero. When the diffusivity exponent a is greater than one, i.e., $a > 1$, the decrease in diffusivity occurs much faster than the rate of solvent removal. Consequently, substantial concentration gradients develop across the film as it dries ($\bar{\phi}_0 \to 0$), suggesting the onset of skin formation. However, when $a \leq 1$, the average gradient remains $O(\varepsilon)$ in size; this is because the film dries before the diffusivity changes enough to induce the formation of a skin.

Figure S4 shows the evolution of the average concentration gradient (S16) that has been computed numerically (lines) and asymptotically (symbols) for two values of a. When $a = 0$, the diffusivity is constant and, as expected, the concentration gradients remain $O(\varepsilon)$ in size. However, when $a = 3$, strong gradients develop across the film when $t \sim 1.5$, which is precisely the time when the rate of thinning begins to decrease in comparison to the rate predicted from the leading-order solution (S14). For both values of a, the asymptotic gradient, as calculated from (S17) and shown as stars, accurately captures the numerical results in stage (ii). The divergence between the asymptotic and numerical solutions at time $t \sim 1.5$ in the case when $a = 3$ is due to a breakdown of the asymptotics, which is now discussed.

The decrease in the diffusivity that occurs within the second stage suggests that it will be possible for the left- and right-hand sides of the diffusion equation (S10a) to attain the same order of magnitude. Physically, this corresponds to the time scales of mass transfer (evaporation) and diffusion becoming commensurate, and it signifies the onset of a third drying stage. Indeed, by balancing the two terms in (S10a), we find that the third stage occurs when $\bar{\phi} \sim \varepsilon^{1/a}$, which is equivalent to $\phi \sim \mathrm{Pe}^{1/a}$. The

height of the film during the transition into the third stage and the time at which this happens can be estimated from (S12) and (S14); this yields

$$\bar{h}_0 \sim (1-\phi_\mathrm{i})/(1-\phi_\mathrm{i}\epsilon^{1/a}) \sim (1-\phi_\mathrm{i})(1+\phi_\mathrm{i}\epsilon^{1/a}) \tag{S18}$$

and $\bar{t}_* \sim \phi_\mathrm{i} - (1-\phi_\mathrm{i})\log[\phi_\mathrm{i}^{-1}(1-\phi_\mathrm{i})\mathrm{Pe}^{1/a}]$, respectively. Since both terms in the diffusion equation (S10a) become similar in magnitude when $\bar{\phi} \sim \varepsilon^{1/a}$, the asymptotic solution that was computed in this subsection ceases to be valid. Thus, the scalings for $\bar{\phi}$ and $\bar{h}_0$ are used to reformulate a model that is valid in the third drying stage.

S4.3 Stage (iii): Skin formation

The relevant small parameter in the third stage is $\phi_\mathrm{i}\varepsilon^{1/a}$, which is equivalent to $\mathrm{Pe}^{1/a}$. Thus, we rescale the variables in the dimensionless model (12) according to $z = (1-\phi_\mathrm{i})\breve{z}$, $t = \bar{t}_* + (1-\phi_\mathrm{i})\breve{t}$, $h = (1-\phi_\mathrm{i})[1+\mathrm{Pe}^{1/a}(1-\phi_\mathrm{i})^{1/a}\breve{h}]$, and $\phi = \mathrm{Pe}^{1/a}(1-\phi_\mathrm{i})^{1/a}\breve{\phi}$. The additional factors in the rescaling that are proportional to $(1-\phi_\mathrm{i})$ are for mathematical convenience; they do not represent additional space and time regimes. Taking $\mathrm{Pe} \to 0$ with $\delta\,\mathrm{Pe}^{-1} = O(1)$ yields a simplified leading-order model that describes the drying process in the third stage. This is given by

$$\frac{\partial\breve{\phi}}{\partial\breve{t}} = \frac{\partial}{\partial\breve{z}}\left(\breve{D}(\breve{\phi})\frac{\partial\breve{\phi}}{\partial\breve{z}}\right), \tag{S19a}$$

where $\breve{D}(\breve{\phi}) = \breve{\phi}^a + \breve{\delta}$ with $\breve{\delta} = \mathrm{Pe}^{-1}(1-\phi_\mathrm{i})^{-1}\delta$, and the boundary conditions are

$$\frac{\partial\breve{\phi}}{\partial\breve{z}} = 0, \quad \breve{z} = 0, \tag{S19b}$$

$$-\breve{D}(\breve{\phi})\frac{\partial\breve{\phi}}{\partial\breve{z}} = \breve{\phi}, \quad \breve{z} = 1. \tag{S19c}$$

The leading-order equation for the film thickness reads

$$\frac{\mathrm{d}\breve{h}}{\mathrm{d}\breve{t}} = -\breve{\phi}(1,\breve{t}). \tag{S19d}$$

Initial conditions are obtained by matching to the leading-order asymptotic solutions stage (ii), given by (S12) and (S14), as $\bar{\phi}_0$ becomes of size $O(\mathrm{Pe}^{1/a})$; this gives $\breve{\phi}(\breve{z},0) = (1-\phi_\mathrm{i})^{-1/a}$ and $\breve{h}(0) = (1-\phi_\mathrm{i})^{-1/a}$. Due to nonlinear diffusion entering the leading-order governing equations (S19), it is difficult to make analytical progress on this problem; therefore, numerical simulations are used to probe the dynamics in this stage.

The circles in Figure S4 denote the average concentration gradient that is computed from a numerical simulation of (S19). The solution in stage (iii) captures the generation of large concentration gradients on $O(1)$ time scales and their subsequent reduction. The small initial differences between the average concentration gradient that is computed from the full model (12) and the simplified model in the third stage (S19) is due to the matching condition corresponding to a solvent fraction that is spatially uniform. Resolving this initial discrepancy is possible by matching higher-order asymptotic solutions in stages (ii) and (iii).

S4.4 Stage (iv): Final drying

The fourth drying stage is entered when the solvent fraction is sufficiently small that the diffusivity can be treated as constant. This occurs when $\breve{\phi} \ll \breve{\delta}^{1/a}$ or, in terms of the original variables, when $\phi \ll \delta^{1/a}$. The governing equations in stage (iv) can be derived from those in stage (iii) by taking the limit as $\breve{\phi} \to 0$ with $\breve{h} = O(\breve{\phi})$ of (S19). This yields a linear system of equations given by

$$\frac{\partial\breve{\phi}}{\partial\breve{t}} = \breve{\delta}\frac{\partial^2\breve{\phi}}{\partial\breve{z}^2}, \tag{S20a}$$

which is supplemented with boundary conditions

$$\frac{\partial \breve{\phi}}{\partial \breve{z}} = 0, \quad \breve{z} = 0, \tag{S20b}$$

$$-\breve{\delta}\frac{\partial \breve{\phi}}{\partial \breve{z}} = \breve{\phi}, \quad \breve{z} = 1. \tag{S20c}$$

The film thickness is given by

$$\frac{\mathrm{d}\breve{h}}{\mathrm{d}\breve{t}} = -\breve{\phi}(1, \breve{t}). \tag{S20d}$$

The initial conditions for this problem can, in principle, be obtained by matching to the solution in stage (iii); however, they will not be required. The solution to (S20) can easily be found via a Fourier series and written as

$$\breve{\phi}(\breve{z}, \breve{t}) = \sum_{n=0}^{\infty} \breve{A}_n \exp(-\lambda_n^2 \breve{\delta}\breve{t}) \cos(\lambda_n \breve{z}), \tag{S21}$$

where the Fourier coefficients $\breve{A}_n$ are determined from matching conditions and the eigenvalues λ_n satisfy the transcendental equation

$$\lambda_n \tan(\lambda_n) = \breve{\delta}^{-1}, \tag{S22}$$

which results from imposing the boundary condition (S20c). The eigenvalues are ordered according to their magnitude as $\lambda_0^2 < \lambda_1^2 < \ldots < \lambda_n^2$ as $n \to \infty$. The film thickness can be found by inserting the solution (S21) into (S20d), integrating with respect to time, and using the fact that $\breve{h} \to 0$ as $\breve{t} \to \infty$ since the scaling of the film thickness in stage (iii) implies that $\breve{h}$ represents the departure from the steady-state thickness $h_\infty = 1 - \phi_\mathrm{i}$; see Section S4.3. We find that

$$\breve{h}(\breve{t}) = \sum_{n=0}^{\infty} \breve{A}_n \lambda_n^{-1} \sin(\lambda_n) \exp(-\lambda_n^2 \breve{\delta}\breve{t}). \tag{S23}$$

For sufficiently large times, the first term in the sum in (S23) will dominate so that in the final stages of drying, the film thickness decreases exponentially in time according to

$$\breve{h}(\breve{t}) \sim \breve{A}_0 \lambda_0^{-1} \sin(\lambda_0) \exp(-\lambda_0^2 \breve{\delta}\breve{t}), \tag{S24}$$

thus implying that the final rate of thinning is set by the dimensionless parameter $\breve{\delta}$ and independent of the exponent a in the diffusivity. Furthermore, from (S24) we see that

$$\frac{\mathrm{d}}{\mathrm{d}\breve{t}}\left[\log \breve{h}(\breve{t})\right] \sim -\lambda_0^2 \breve{\delta}. \tag{S25}$$

S5 Asymptotic analysis of solvent absorption in the limit of strong saturation

When analysing the problem of solvent absorption, it is convenient to rescale the solvent fraction in the non-dimensional model (12) according to $\phi = \phi_\mathrm{e}\Phi$ so that $\Phi = 1$ corresponds to the equilibrium saturation. In this case, the diffusion equation can be written as

$$\frac{\mathrm{Pe}}{\phi_\mathrm{e}^a}\frac{\partial \Phi}{\partial t} = \frac{\partial}{\partial z}\left(\mathcal{D}(\Phi)\frac{\partial \Phi}{\partial z}\right), \tag{S26a}$$

where $\mathcal{D}(\Phi) = \Phi^a + \Delta$ with $\Delta = \delta\phi_\mathrm{e}^{-a}$, which has boundary conditions given by

$$\frac{\partial \Phi}{\partial z} = 0, \qquad z = 0, \tag{S26b}$$

$$-\mathcal{D}(\Phi)\frac{\partial \Phi}{\partial z} = \frac{\mathrm{Pe}}{\phi_\mathrm{e}^a}(1 - \phi_\mathrm{e}\Phi)(\Phi - 1), \quad z = h(t). \tag{S26c}$$

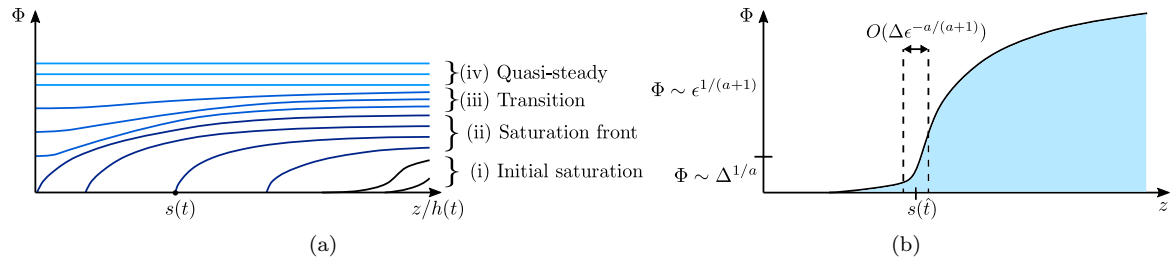


Figure S5: (Color online) The dynamics of solvent absorption in the limit of strong saturation, $\epsilon \equiv \mathrm{Pe}\,\phi_{\mathrm{e}}^{-a} \ll 1$. (a) A simplified schematic diagram depicting the evolution of the solvent fraction in four key stages. (b) Detailed image of the asymptotic structure of the solution in the second stage where there is a saturation front that propagates from the film surface towards the substrate.

The film expands according to

$$\frac{\mathrm{d}h}{\mathrm{d}t} = \phi_{\mathrm{e}}\left[1 - \Phi(h(t), t)\right]. \tag{S26d}$$

The initial conditions are

$$\Phi = 0, \quad h = 1, \quad t = 0. \tag{S26e}$$

In the case of strong saturation, defined by $\epsilon \equiv \mathrm{Pe}\phi_{\mathrm{e}}^{-a} \ll 1$, there are four key stages to consider, which are summarised in Figure S5 (a).

S5.1 Stage (i): Initial saturation

This stage describes the initial saturation of the film which is confined to a thin boundary layer near the surface. Stage (i) can, in fact, be decomposed into two sub-stages. In the first sub-stage, the solvent fraction is sufficiently small that the diffusivity is approximately constant. In the second, the solvent fraction is still small but the diffusivity begins to vary.

To proceed with the analysis in the first sub-stage, a small parameter $\mu \ll \Delta^{1/a}$ is introduced and used to scale the solvent fraction and the diffusivity as $\Phi \sim \mu$ and $\mathcal{D} \sim \Delta$, respectively. Balancing terms in the boundary condition (S26c) requires that $h(t) - z \sim (\Delta/\epsilon)\mu$, while balancing terms in the diffusion equation (S26a) then gives a time scale of $t \sim (\Delta/\epsilon)\mu^2$. Thus, we write $\Phi = \mu\bar{\Phi}$, $t = (\Delta/\epsilon)\mu^2\bar{t}$, $z = h(t) - (\Delta/\epsilon)\mu\bar{z}$ in the governing equations (S26) and then take $\mu \to 0$ to obtain the leading-order problem given by

$$\frac{\partial\bar{\Phi}}{\partial\bar{t}} = \frac{\partial^2\bar{\Phi}}{\partial\bar{z}^2}, \tag{S27a}$$

subject to the following boundary and initial conditions:

$$\frac{\partial\bar{\Phi}}{\partial\bar{z}} = -1, \quad \bar{z} = 0, \tag{S27b}$$

$$\bar{\Phi} \to 0, \quad \bar{z} \to \infty, \tag{S27c}$$

$$\bar{\Phi} = 0, \quad \bar{t} = 0. \tag{S27d}$$

Condition (S27b) corresponds to the leading-order part of (S26c), while (S27c) represents the far-field decay of the solvent fraction, which is consistent with the boundary-layer approximation of $\bar{\Phi}$ in this stage. The problem given by (S27) is well known can can be solved using a similarity solution of the form $\bar{\Phi} = \bar{t}^{1/2}g(\bar{z}/\bar{t}^{1/2})$, details of which are given by Crank [1]. The solvent fraction at the surface increases according to $\Phi(0,t) \sim (\epsilon t/\Delta)^{1/2}$ which implies that the solution in this sub-stage is valid until $t \sim \Delta^{(2/a)+1}\epsilon^{-1}$.

The second sub-stage is captured by writing $\Phi = \Delta^{1/a}\bar{\bar{\Phi}}$, $t = \Delta^{(2/a)+1}\epsilon^{-1}\bar{\bar{t}}$, and $z = h(t) - \Delta^{(1/a)+1}\epsilon^{-1}\bar{\bar{z}}$ in the governing equations (S26). The leading-order equations in the limit as $\Delta \to 0$

are of the same form as (S27) but have a nonlinear diffusion coefficient given by $\bar{\bar{\mathcal{D}}}(\bar{\Phi}) = \bar{\bar{\Phi}}^a + 1$ and the initial condition (S27d) is replaced with a matching condition. The solution to this problem describes the localised saturation of the film surface when nonlinear diffusion becomes a leading-order effect. In this stage, the expansion of the film is small and film thickness is given by $h(\bar{\bar{t}}) \sim 1 + \Delta^{(2/a)+1}\epsilon^{-1}\phi_{\mathrm{e}}\bar{\bar{t}}$.

S5.2 Stage (ii): Saturation front

As the film continues to absorb solvent, the solvent fraction near the surface will exceed magnitudes of $O(\Delta^{1/a})$. However, for sufficiently short times, the solvent fraction will still be far from its equilibrium value, i.e., $\Phi \ll 1$. These two conditions define the second saturation stage. A new scale for the solvent fraction can be obtained by balancing terms in the boundary condition (S26c) assuming that $h(t) - z = O(1)$ and $\Delta^{1/a} \ll \Phi \ll 1$; this yields $\Phi \sim \epsilon^{1/(a+1)}$. Using the scale for Φ in the diffusion equation (S26a) enables a time scale for this stage to be determined, i.e., $t \sim \epsilon^{1/(1+a)}$. The solvent fraction can still be comparatively small, i.e., of size $O(\Delta^{1/a})$, in regions that are sufficiently far from the film surface. Therefore, the spatial domain can be decomposed into two main regions where either $\Phi = O(\Delta^{1/a})$ or $\Phi = O(\epsilon^{1/(a+1)})$, and we will show that these regions are connected by a thin transition layer of width $O(\Delta\epsilon^{-a/(a+1)})$ located at $z = s(t)$, as illustrated in Figure S5 (b). In physical terms, these two spatial regions are located ahead of and behind a saturation front centred at $z = s(t)$ that propagates towards the substrate from the film surface.

We first analyse the region behind the saturation front defined by $s(t) < z < h(t)$ where $\Phi \sim \epsilon^{1/(a+1)}$. Thus, we rescale the variables in the governing equations (S26) according to $\Phi = \epsilon^{1/(a+1)}\hat{\Phi}$, $h = \hat{h}$, and $t = \epsilon^{1/(a+1)}\hat{t}$ and then take the limit as $\Delta \to 0$ to obtain the model given by

$$\frac{\partial \hat{\Phi}}{\partial \hat{t}} = \frac{\partial}{\partial z}\left(\hat{\Phi}^a \frac{\partial \hat{\Phi}}{\partial z}\right), \tag{S28a}$$

which has boundary conditions given by

$$\hat{\Phi} \sim 0, \qquad z \sim s(\hat{t}), \tag{S28b}$$

$$-\hat{\Phi}^a \frac{\partial \hat{\Phi}}{\partial z} = \left(1 - \phi_{\mathrm{e}}\epsilon^{1/(a+1)}\hat{\Phi}\right)\left(\epsilon^{1/(a+1)}\hat{\Phi} - 1\right), \quad z = \hat{h}(\hat{t}). \tag{S28c}$$

The no-flux condition at the substrate given by (S26b) has been replaced by a matching condition stating that the solvent fraction asymptotically tends to zero as the transition layer is approached. The evolution equation for the film thickness is

$$\frac{\mathrm{d}\hat{h}}{\mathrm{d}\hat{t}} = \epsilon^{1/(a+1)}\phi_{\mathrm{e}}\left[1 - \epsilon^{1/(a+1)}\hat{\Phi}(h(\hat{t}), \hat{t})\right]. \tag{S28d}$$

Matching conditions for the film thickness are given by $\hat{h} \sim 1$ as $\hat{t} \sim 0$. The film thickness can, therefore, be written as

$$\hat{h}(\hat{t}) = 1 + \epsilon^{1/(a+1)}\phi_{\mathrm{e}}\hat{t} + O(\epsilon^{2/(a+1)}). \tag{S29}$$

A matching condition for $\hat{\Phi}$ as $\hat{t} \sim 0$ will not be required.

We now examine the leading-order part (in $\epsilon^{1/(a+1)}$) of (S28), which is given by

$$\frac{\partial \hat{\Phi}}{\partial \hat{t}} = \frac{\partial}{\partial z}\left(\hat{\Phi}^a \frac{\partial \hat{\Phi}}{\partial z}\right), \tag{S30a}$$

with boundary conditions

$$\hat{\Phi} \sim 0, \quad z \sim s(\hat{t}), \tag{S30b}$$

$$\hat{\Phi}^a \frac{\partial \hat{\Phi}}{\partial z} = 1, \quad z = 1, \tag{S30c}$$

where we have used the fact that $\hat{h}(\hat{t}) = 1 + O(\epsilon^{1/(a+1)})$; see (S29). An equation for the position of the saturation front s can be deduced by integrating (S30a) between $z = s$ and $z = 1$ and using the conditions (S30b), (S30c), and $s(0) = 1$ to obtain

$$\int_{s(\hat{t})}^{1} \hat{\Phi}(z, \hat{t})\, \mathrm{d}z = \hat{t}. \tag{S31}$$

Counting the degrees of freedom reveals that the solution in the region behind the saturation front is fully determined by the system of equations (S30a)–(S31). Furthermore, by introducing the change of variable $z = 1 - \hat{z}$ and setting $s(\hat{t}) = 1 - \hat{s}(\hat{t})$, it can be shown that (S30a)–(S31) admits a self-similar solution of the form

$$\hat{\Phi}(\hat{z}, \hat{t}) = \hat{t}^{1/(a+2)} f\left(\frac{\hat{z}}{\hat{t}^{(a+1)/(a+2)}}\right), \quad \hat{s}(\hat{t}) = S\hat{t}^{(a+1)/(a+2)}, \tag{S32}$$

where f satisfies the free boundary value problem given by

$$-\left(\frac{a+1}{a+2}\right)\xi \frac{\mathrm{d}f}{\mathrm{d}\xi} + \frac{1}{a+2} f(\xi) = \frac{\mathrm{d}}{\mathrm{d}\xi}\left[f^a(\xi)\frac{\mathrm{d}f}{\mathrm{d}\xi}\right], \tag{S33a}$$

with

$$-f^a \frac{\mathrm{d}f}{\mathrm{d}\xi} = 1, \quad \xi = 0, \tag{S33b}$$

$$f \sim 0, \quad \xi \sim S, \tag{S33c}$$

where the similarity variable ξ is defined as

$$\xi = \hat{z}/(\hat{t}^{(a+1)/(a+2)}). \tag{S33d}$$

The free boundary S is determined from the condition

$$\int_0^S f(\xi)\, \mathrm{d}\xi = 1. \tag{S33e}$$

In general, solutions to (S33) have to be computed numerically. However, it is possible to obtain a local solution that is valid close to the saturation front given by

$$f(\xi) \sim \left[\frac{Sa(a+1)}{a+2}(S - \xi)\right]^{1/a}, \quad \xi \to S^-. \tag{S34}$$

A comparison of the local solution (S34) with numerical solutions of (S33), shown in Figure S6 (a), reveals that the local solution is an excellent approximation to the true solution even at points that are far from the saturation front. The local solution (S34) implies that the solvent fraction near the front is given by

$$\Phi \sim \epsilon^{1/(a+1)} \left[\frac{a(a+1)}{a+2}\frac{(1 - s(\hat{t}))}{\hat{t}}\left(z - s(\hat{t})\right)\right]^{1/a} \tag{S35}$$

as $z \sim s(\hat{t})^+$, which will be useful when matching to the solution in the transition layer. Using the local solution (S34) in the integral (S33e), we find that the free boundary S is given approximately by

$$S \simeq \left[\frac{(a+1)^{a-1}(a+2)}{a^{a+1}}\right]^{1/(a+2)}, \tag{S36}$$

which agrees remarkably well with numerically computed values, as shown in Figure S6 (b).

The region ahead of the saturation front and the thin transition layer can be analysed together. Recalling that the transition layer is characterised by the size of the solvent fraction, i.e., $\Phi \sim \Delta^{1/a}$, and the time scale has been set by considering the dynamics in the region behind the front, i.e., $t \sim \epsilon^{1/(a+1)}$,

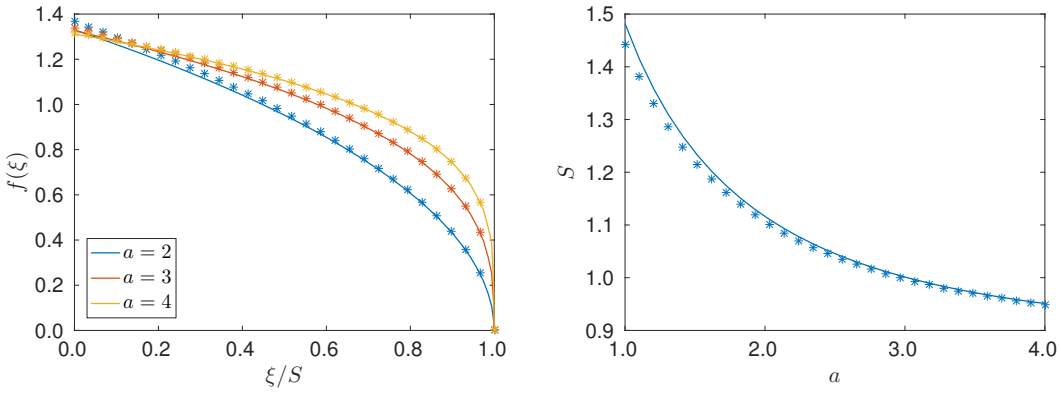


Figure S6: (Color online) (a) Self-similar profiles of the solvent fraction in the strong-saturation limit, plotted as functions of a similarity variable $\xi = (1-z)/\hat{t}^{(a+1)/(a+2)}$ for various values of the diffusivity exponent a. The position of the saturation front is given by $1-s(t) = S\hat{t}^{(a+1)/(a+2)}$. (b) The dependence of the self-similar front position S as a function of the diffusivity exponent a. In both panels, solid lines represent numerical solutions of the similarity problem; symbols denote quantities obtained from a local solution (S34) valid near the saturation front, i.e., $\xi \sim S^-$.

we rescale variables in the system of equations (S26) according to $\Phi = \Delta^{1/a}\check{\Phi}$, $t = \epsilon^{1/(a+1)}\hat{t}$, and introduce a travelling-wave coordinate ζ defined by $z = s(\hat{t}) + (\Delta\epsilon^{-a/(a+1)})\zeta$. This definition of ζ implies that $\zeta \to -\infty$ and $\zeta \to +\infty$ correspond to regions ahead of and behind the saturation front, respectively. Upon taking the limit as $\Delta\epsilon^{-a/(a+1)} \to 0$, the leading-order part of the diffusion equation (S26a) is given by

$$-\frac{\mathrm{d}s}{\mathrm{d}\hat{t}}\frac{\partial\check{\Phi}}{\partial\zeta} = \frac{\partial}{\partial\zeta}\left[\left(\check{\Phi}^a + 1\right)\frac{\partial\check{\Phi}}{\partial\zeta}\right]. \tag{S37}$$

We shall assume that the solvent fraction far ahead of the saturation front is small so that $\check{\Phi} \to 0$ as $\zeta \to -\infty$. Moreover, to remove the translational invariance of the problem, we set $\check{\Phi} = 1$ at $\zeta = 0$. The solution to (S37) can be written in an implicit form and upon applying the boundary conditions we find that

$$\frac{1}{a}\check{\Phi}^a + \log\check{\Phi} = \frac{1}{a} - \frac{\mathrm{d}s}{\mathrm{d}\hat{t}}\,\zeta. \tag{S38}$$

Far ahead of the front, i.e., when $\zeta \ll -1$ and $\log\check{\Phi} \gg \check{\Phi}^a$, we find that $\check{\Phi} \sim \exp(-\dot{s}\zeta)$, where $\dot{s} = \mathrm{d}s/\mathrm{d}\hat{t}$, corresponding to the usual Fickian travelling-wave profile found in problems with constant diffusivity. Far behind the front, i.e., when $\zeta \gg 1$ and $\log\check{\Phi} \ll \check{\Phi}^a$, we have that $\check{\Phi} \sim (-a\dot{s}\zeta)^{1/a}$, which can be written as $\Phi \sim \epsilon^{1/(a+1)}[-a\dot{s}(z - s(\hat{t}))]^{1/a}$. Matching this far-field solution to (S35) implies that $\dot{s} = -[(a+1)/(a+2)](1-s)/\hat{t}$. This equation has the solution $s(\hat{t}) = 1 - S\hat{t}^{(a+1)/(a+2)}$, which is consistent with the similarity solution that was computed in the region behind the front (S32).

An example of the solvent fraction in stage (ii) is shown in Figure S7. The line represents a numerical solution of (S30) that uses the full form the diffusivity given by $\hat{\mathcal{D}}(\hat{\Phi}) = \hat{\Phi}^a + \Delta\epsilon^{-a/(a+1)}$ and replaces the matching condition at the saturation front (S30b) with the original no-flux condition at the substrate, $\partial\hat{\Phi}/\partial z = 0$ at $z = 0$. The dashed line corresponds to the similarity solution behind the saturation front (S32) and the stars are the asymptotic solution in the transition layer (S38). The asymptotic solutions are in excellent agreement with the numerical solution. In physical terms, the similarity solution corresponds to the propagation of a *sharp* saturation front that separates regions of the film that are partially saturated ($\hat{\Phi} > 0$) from those which are completely dry ($\hat{\Phi} = 0$). The asymptotic solution in the transition layer accounts for the small, but non-zero, value of the diffusivity in the dry region of the film and describes the consequent broadening of the sharp front. Thus, the transition layer can be thought of as a *diffuse* saturation front whose thickness tends to zero in the limit as $\Delta \to 0$.

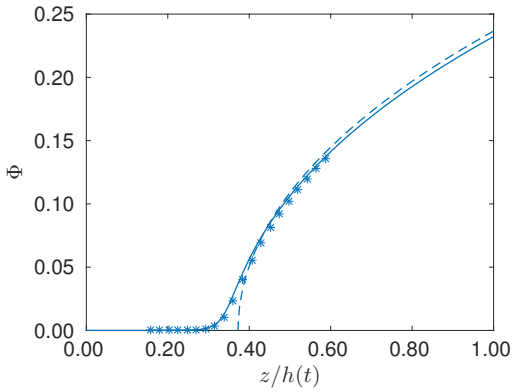


Figure S7: (Color online) A comparison of the numerical (solid line) and asymptotic (stars and dashed line) solution of the solvent fraction in stage (ii) of the strong-saturation problem. Behind the saturation front, i.e., for $z/h(t) > 0.37$, the solvent fraction is well described by the similarity solution (dashed line) obtained from (S33). Stars denote the leading-order solution (S38) in the transition layer that connects regions ahead and behind the saturation front at $z/h(t) \simeq 0.37$. Parameters are $\delta = 10^{-5}$, $a = 2$, $\phi_e = 10^{-1}$, $\mathrm{Pe} = 10^{-4}$, and $\phi_i = 0$. The solution is shown at time $t = 10^{-1}$.

The asymptotic solutions that have been computed in stage (ii) will fail to remain valid if either the saturation front reaches the substrate, or the solvent fraction near the surface becomes close to its equilibrium value. The time at which the surface begins to approach equilibrium can be estimated as $\hat{t}_{\mathrm{sat}} \sim \epsilon^{-(a+2)/(a+1)}$, assuming that $f(0) = O(1)$. The saturation front will reach the substrate when $s(\hat{t}_{\mathrm{sub}}) \sim 1$, which implies that $\hat{t}_{\mathrm{sub}} \sim 1$, where it has been assumed that $S = O(1)$. Due to the assumption that $\epsilon \ll 1$, the saturation front will always reach the substrate before equilibrium saturation is obtained near the surface, i.e., $\hat{t}_{\mathrm{sub}} \ll \hat{t}_{\mathrm{sat}}$. This fact is used to define a third stage describing the dynamics that occur after the saturation front coincides with the substrate.

S5.3 Stage (iii): Transition

The subsequent evolution of the system upon the saturation front reaching the substrate can be described by (S30a) and (S30c) with the matching condition (S30b) replaced with the original no-flux condition (S26b) and an initial condition given by $\hat{\Phi}(z, \hat{t}_{\mathrm{sub}}) \simeq f(S(1-z))$. Although a closed-form solution to this problem was not obtained, it is possible to show that

$$\hat{\Phi} \sim \hat{t} \tag{S39}$$

for $1 \ll \hat{t} \ll \epsilon^{-1/(a+1)}$ using an approach similar to that in Section S4.1. Thus, the solvent profile flattens and the concentration of solvent becomes uniform throughout the film.

S5.4 Stage (iv): Quasi-steady

The long-term approximate solution for the solvent fraction given by (S39) and the solution for the film thickness (S29) can be used to match into a new time stage where $\hat{\Phi} = O(\epsilon^{-1/(a+1)})$ and $\hat{t} = O(\epsilon^{-1/(a+1)})$. This scaling results in the original governing equations given by (S26) with $\mathrm{Pe}\,\phi_e^{-a}$ replaced with ϵ and the initial conditions (S26e) replaced with matching conditions given by $\Phi \sim t$ and $h \sim 1 + \phi_e t$ when $t = O(\epsilon^{1/(a+1)})$; these matching conditions result from (S39) and (S29), respectively. Due to the assumption that $\epsilon \ll 1$ and the limitations on the smallness of Φ and t from the matching conditions, diffusion will occur on a much smaller time scale than absorption of solvent from the surrounding atmosphere. Thus, the solvent fraction will evolve quasi-statically. The solution to (S26) in stage (iv) can be obtained as a regular asymptotic expansion of the form $\Phi \sim \Phi_0 + \epsilon\Phi_1$ and $h \sim h_0 + \epsilon h_1$. As in the second stage of the drying problem (see Section S4.2), the $O(1)$ problem simply states that the leading-order solution for the solvent fraction is uniform in space. By solving the $O(\epsilon)$ problem, we find that $\Phi_0(z,t) \equiv \phi_e^{-1}[1 - 1/h_0(t)]$,

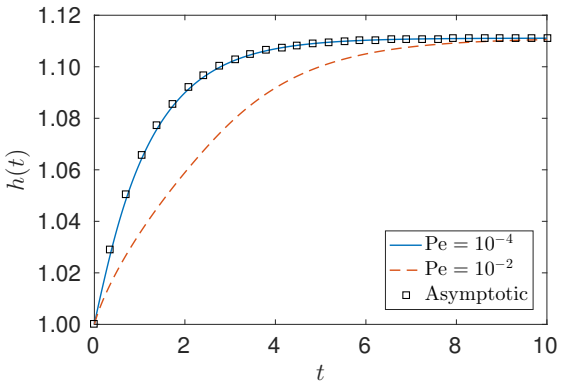


Figure S8: (Color online) Evolution of the film thickness. The lines represent numerical solutions of (12) and the symbols correspond to the asymptotic solution (19). Parameters are $\delta = 10^{-5}$, $a = 2$, $\phi_e = 10^{-1}$, and $\phi_i = 0$.

where the leading-order film thickness h_0 satisfies

$$\frac{\mathrm{d}h_0}{\mathrm{d}t} = -(1-\phi_e) + \frac{1}{h_0}, \tag{S40}$$

with $\Phi_0 = 0$ and $h_0 = 1$ as $t = 0$. The implicit solution to (S40) that satisfies the initial conditions can be written as

$$h_0 - 1 + \frac{1}{1-\phi_e}\log\left[\frac{1-(1-\phi_e)h_0}{\phi_e}\right] = -(1-\phi_e)t. \tag{S41}$$

A comparison of the asymptotic solution for the film thickness given by (S41) with a numerical solution of the full model (12) is shown in Figure S8. The exceptional agreement between these two solutions provides verification that, despite the complicated dynamics that occur in stages (i)–(iii), the film thickness is mainly driven by the relatively simple quasi-steady dynamics of stage (iv).

S6 Fitting of absorption experiments at fixed relative humidity

Table S1: Experimental data from film sorption experiments at 20% RH for mixtures with different initial glycerol fractions. The equilibrium volume fraction ϕ_e has been computed using two methods based on the final film thickness. In the "exact" approach, (13) is inverted to give $\phi_e = 1 - (h_\infty/h_i)^{-1}$. In the "approximate" approach, the smallness of $h_\infty/h_i - 1$ is exploited to write $\phi_e \simeq h_\infty/h_i - 1$. The time scale of absorption $\tau_{abs} = h_i/k$ is calculated by fitting the data to the master curve (21) using the approximate value of ϕ_e for consistency.

Glycerol fraction	h_∞/h_i	ϕ_e (exact)	ϕ_e (approx)	τ_{abs} [min]
0	1.08	0.072	0.077	3.15
0.02	1.05	0.049	0.052	24.6
0.04	1.03	0.027	0.027	46.9
0.06	1.04	0.038	0.040	24.7
0.08	1.04	0.041	0.043	32.8
0.10	1.06	0.059	0.063	20.2
0.15	1.03	0.026	0.027	42.4

References

[1] J. Crank. *The Mathematics of Diffusion.* Oxford University Press, 1979.

[2] I. Hadj Romdhane, P. E. Price, C. A. Miller, P. T. Benson, and S. Wang. Drying of glassy polymer films. *Ind. Eng. Chem. Res.*, 40(14):3065–3075, 2001.

[3] M. G. Hennessy and A. Münch. Dynamics of a slowly evaporating solvent-polymer mixture with a deformable upper surface. *IMA J. Appl. Math.*, 79(4):681–720, 2014.

[4] P. E. Price, S. Wang, and I. Hadj Romdhane. Extracting effective diffusion parameters from drying experiments. *AIChE J.*, 43(8):1925–1934, 1997.

[5] J. S. Vrentas and C. M. Vrentas. Drying of solvent-coated polymer films. *J. Polym. Sci. Poly. Phys*, 32(1):187–194, 1994.